




Magnetically controllable photon blockade under a weak quantum-dot–cavity coupling conditionShuting Shen ^{*}, Jiahua Li [†], and Ying Wu [‡]*School of Physics, Huazhong University of Science and Technology, Wuhan 430074, People's Republic of China*

(Received 25 October 2019; accepted 21 January 2020; published 5 February 2020)

Quantum control of photons has become an area of great interest in the development of quantum technology. Here we explore how an external magnetic field can be exploited to control the statistical properties of photons in a bimodal cavity quantum electrodynamics (CQED) system. Our CQED system is composed of a bimodal micropillar Fabry-Pérot cavity containing a single V -level quantum dot (QD) involving fine-structure-splitting neutral exciton transitions under the effect of the applied magnetic field in the presence of an incident pump laser field driving one cavity mode. With the introduction of the external magnetic field, not only is the conversion of polarization characteristics of photons achieved, but the statistics properties of photons are well engineered and the switching between photon bunching and antibunching is realized in the weak-coupling regime of CQED. The superiority of our system is manifested in the following aspects. (i) Using experimental parameters, we can manipulate the statistical properties of photons by appropriately tuning the strength of the magnetic field under the weak-coupling CQED condition, accompanied by either enhanced antibunching or a transition from antibunching to strong bunching of the light and vice versa. So we can arrive at selective photon statistics. (ii) The strong photon antibunching effect, under nonresonant scenarios but without the need to match the resonant or near-resonant conditions for the cavity and QD, can appear. Furthermore, we find that the multifrequency photon blockade can be generated in the present system, which is different from previous studies about photon blockade only for specific optical detuning. (iii) The high photon occupations or transmissions, simultaneously accompanied by strong photon antibunching in the system, are beneficial to the correlation measurement in practical experiments. This process works with a high quality of photon antibunching and bunching over a wide range of parameters and has potential applications in on-chip quantum information processing. It is hoped that the proposed scheme provides a possibility for the generation of tunable single-photon sources or controllable photon quantum gates.

DOI: [10.1103/PhysRevA.101.023805](https://doi.org/10.1103/PhysRevA.101.023805)**I. INTRODUCTION**

In recent decades, cavity quantum electrodynamics (CQED) of solid-state systems [1,2] consisting of a single neutral or charged semiconductor quantum dot (QD) and an optical microcavity have attracted considerable attention due to their broad application prospects in, e.g., quantum light sources [3,4], quantum communication, and quantum computing [5,6]. A substantial number of works have been focused on achieving fundamental CQED effects in solid-state systems, including the Purcell effect [7], vacuum Rabi splitting, and the Jaynes-Cummings (JC) ladder effect in a variety of coupled QD-cavity systems. According to the coupling strength between the emitter and the cavity, the coupled QD-cavity systems can be classified into two different regions: One is the weak-coupling CQED regime and the other is the strong-coupling CQED regime. Specifically, in the weak-coupling CQED regime where the coupling strength between the emitter and the cavity mode is much lower than the dissipation rate, the system can exhibit the Purcell effect, namely, the

spontaneous emission rate of the QD can be modified due to the exciton-photon interaction [8]. Contrarily, in the strong-coupling CQED regime where the coupling strength between the QD and the cavity mode is greater than the dissipation rate, a reversible exchange of energy between the QD and the cavity mode gives rise to Rabi oscillations and Rabi splittings [1,2,9,10]. Among them, a two-level QD-cavity coupling system constitutes the JC model. Interestingly, the anharmonic JC ladder leads to attractive optical phenomena [11–13], for example, photon antibunching and photon bunching, which have important applications in the generation of nonclassical light [14]. In photon antibunching, the coupling between a single photon and a system impedes the coupling of subsequent photons [15]. On the contrary, in photon bunching, the coupling of initial photons is beneficial to the coupling of subsequent photons. In the strong-coupling regime of CQED, photon antibunching has been illustrated in various of optical systems, such as CQED systems [14,16–20], circuit quantum electrodynamics systems [21–24], waveguide QED systems [25–27], optomechanical systems [28–38], spinning or gain resonator systems [39–41], and so on.

Following the photon antibunching effect in the strong-coupling region, the photon antibunching effect based on the destructive quantum interference between different excitation paths arises, which greatly reduces the requirement of strong nonlinearity of the system. This phenomenon is called un-

^{*}shenst1995@163.com[†] Author to whom correspondence should be addressed:

huajia_li@163.com

[‡]yingwu2@126.com

conventional photon antibunching, which has been studied in, e.g., two directly coupled cavities with second-order or third-order (Kerr) optical nonlinearity [42–53], two coupled superconducting circuit resonators [54], coupled cavity optomechanical systems [55–59], and CQED systems [60–64]. More recently, a scheme to enhance photon antibunching by the quantum interference effect in a three-level Δ configuration has been proposed [65], which provides a possibility for single-photon generation by unconventional photon antibunching.

With further studies of solid-state CQED systems, it was gradually found that the interaction between the QD and the cavity can be controlled not only by the electric field or temperature [66–68], but also by the magnetic field [69–71]. The magnetic field can be introduced to manipulate the QD exciton states, which lifts the degeneracy of exciton states of the QD due to the Zeeman effect [72,73]. Under an external magnetic field, high-fidelity and high-speed spin initialization and manipulation have been studied in a coupled QD bimodal cavity [74] and the interaction between exciton spin states and photon modes has been experimentally realized [75]. However, in the QD-cavity architectures there have been few demonstrations of an external magnetic field being introduced to control the photon statistics characteristics.

Since the applied magnetic field can affect the interaction between the QD exciton transitions and the cavity modes in CQED, a natural question to ask, then, is whether the magnetic field will affect the statistical properties of photons in the cavity. This question arouses our great interest. For this reason, on the basis of the experiments mentioned above [69–75], here we propose a CQED scheme in which a coupled V -level neutral QD–bimodal micropillar cavity system is pumped by an incident laser field under the effect of an external magnetic field. Starting from the expressions of two spin exciton states, i.e., $|\sigma_+\rangle$ and $|\sigma_-\rangle$ (see Fig. 2 below), of the neutral V -level QD, the expressions of two eigenstates, i.e., $|X\rangle$ and $|Y\rangle$, of the neutral V -level QD as well as two orthogonally and linearly polarized exciton states, i.e., $|H\rangle$ and $|V\rangle$, are given step by step, in which the directions of two orthogonally and linearly polarized exciton states $|H\rangle$ and $|V\rangle$ are identical to those of two orthogonally and linearly polarized cavity modes, i.e., a_H and a_V . The orthogonally and linearly polarized exciton states $|H\rangle$ and $|V\rangle$ are respectively coupled to the orthogonal cavity modes a_H and a_V of the bimodal micropillar cavity according to selection rules. Then a quantum master equation is introduced to simulate the intracavity photon response of the CQED system including photon occupations and statistics. It is found that by tuning the magnetic field appropriately, the photon statistics properties of the system can be well controlled in the weak-coupling “bad cavity” regime. In particular, the photon statistics is revealed to be capable of switching from antibunched photons to bunched photons or vice versa by tuning the external magnetic field. Thus we can achieve selective photon statistics. Our in-depth results indicate that introducing an external magnetic field offers a highly sensitive method (or a new degree of freedom) for manipulating quantum states. We also find that the V -polarized photons produced by the intermediate modulation of the magnetic field and the coherent coupling via the terms $i\beta(|H\rangle\langle V| - |V\rangle\langle H|)$ and $\Delta_{FS} \sin \theta \cos \theta(|H\rangle\langle V| + |V\rangle\langle H|)$ [see Eq. (14) below]

have the characteristics of high photon occupations or transmissions, simultaneously accompanied by strong photon antibunching. This can be achieved in our system without needing to construct the cavity-coupling-cavity protocol presented in previous works [76–81]. In addition, our system reduces the requirement of resonance or near resonance between the QD exciton transitions and the cavity modes [61], making it possible to generate strong antibunching in the presence of detuning or out of resonance. At the same time, we observe that the multifrequency photon blockade can be achieved in the present system, which is different from previous studies on photon blockade only for specific laser detuning [42,43]. Also, we explore the dependence of photon antibunching on the other system parameters and the results show that our approach works with high-quality photon antibunching and bunching for a large range of parameters, which increase the feasibility of the experiment.

We note that the photon statistics of the field emitted from a semiconductor optical microcavity containing a solid-state quantum well have been systematically investigated for different scenarios [82,83], for example, in the quantum trajectory approach, in the linear regime, in the nonlinear regime, and in the nonstationary regime. Reference [82] revealed interesting dynamical behaviors of the autocorrelation function depending on the system parameters. In Ref. [83] the analytical expressions of the light-emitting autocorrelation function in the weak pumping field were derived for the two coupling regimes (the weak-coupling regime and the strong-coupling regime) and statistical similarities of the photon to an atomic cavity were discussed. To date, studies of the photon statistics in a bimodal CQED system with a three-level QD and an external magnetic field are lacking.

The remainder of the paper is organized as follows. In Sec. II we describe the physical model of the CQED system under consideration and gradually give the total Hamiltonian in terms of both the linearly polarized exciton states and the linearly polarized cavity modes (Sec. II A). Subsequently, the quantum master equation governing the CQED system is yielded (Sec. II B). We further introduce the second-order intensity correlation function which provides key information on the photon statistics (Sec. II C). In Sec. III, starting from a Schrödinger equation approach, an analytical discussion for the second-order correlation function of the CQED system is presented. In Sec. IV we discuss and analyze the statistical properties of the V -polarized photons as an example by varying the strength of the external magnetic field under the weak-coupling condition, where the requirement for a perfectly matched QD cavity can be relaxed in favor of photon-blockade optimization. After this, we look into the dependence of the photon antibunching characteristics on the other system parameters. Finally, we summarize our results in Sec. V.

II. BASIC FRAMEWORK OF THE SYSTEM

A. Model and Hamiltonian

As depicted schematically in Fig. 1, the CQED system considered here is composed of a bimodal cavity containing a single self-assembled neutral QD under the effect of an external magnetic field in the Faraday configuration, where

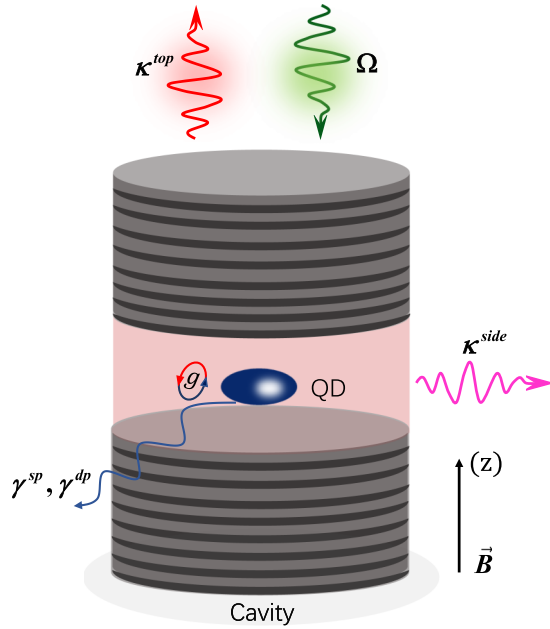


FIG. 1. Schematic of the cavity-QD system under consideration. A single self-assembled neutral QD is coupled to an elliptical micropillar cavity with two linearly polarized modes, i.e., the H and V modes, at coupling rates g_H and g_V under the effect of an external magnetic field B applied in the growth direction of the embedded QD, i.e., the Faraday geometry. An incident pump laser field Ω is polarized along the H -polarized cavity mode axis. Here κ^{top} is the top-mirror damping rate, corresponding to the cavity photons, to escape the cavity through the top port and κ^{side} is the side-leakage damping rate induced by the micropillar sidewall roughness. The total cavity damping rate is given by the sum $\kappa = \kappa^{\text{top}} + \kappa^{\text{side}}$. Here γ^{sp} and γ^{dp} are the spontaneous emission decay rate and the pure dephasing rate of the QD excitons, respectively.

the magnetic field is applied parallel to the growth direction of the embedded QD. The bimodal cavity considered in our system is an elliptical micropillar Fabry-Pérot cavity which has the same function as the photonic crystal cavity and which can support two orthogonally and linearly polarized cavity modes due to a small ellipticity of the cavity cross section and the material birefringence [84]: One is the H -polarized cavity mode (denoted by a_H) and the other is the V -polarized cavity mode (denoted by a_V). The cavity modes are not directly coupled to each other due to their orthogonal polarizations, and only one cavity mode is driven by an external monochromatic continuous-wave (cw) pump laser field (denoted by Ω) via setting the input polarization. The QD is coherently coupled to these two linearly polarized cavity modes a_H and a_V .

On the other hand, in semiconductor neutral QD systems, one electron in the conduction band and one hole in the valence band bind to form exciton through their mutual Coulombic interaction. Because the energy splitting between the heavy-hole and light-hole states caused by the strain in self-assembled QDs is much larger than the interaction energy of fine structures, it is safe to consider only heavy-hole states and neglect light-hole states [73]. Under the premise of single occupation of each band, four exciton states are constructed on the basis of a heavy-hole valence band with $J_h = 3/2$ and

$J_{h,z} = \pm 3/2$ and an electron conduction band with $S_e = 1/2$ and $S_{e,z} = \pm 1/2$. Here $J_h = 3/2$ ($S_e = 1/2$) represents the spin angular momentum of the heavy-hole valence band (the electron conduction band) and $J_{h,z} = \pm 3/2$ ($S_{e,z} = \pm 1/2$) represents the projection of the angular momentum in the z direction of the heavy-hole valence band (the electron conduction band). These states are classified by the total angular momentum projection along the z axis, namely, $J_z = J_{h,z} + S_{e,z}$. Two of the four exciton states with $J_z = \pm 1$ are bright exciton states that are optically active and can couple to the laser field; the other two with $J_z = \pm 2$ are dark exciton states that are optically inactive and cannot couple to the laser field. The magnetic field introduced in our CQED system is in a Faraday configuration with the orientation of the magnetic field along the heterostructure growth direction (z) rather than in a Voigt configuration with the orientation of the magnetic field perpendicular to the growth direction (in-plane), which results in just opening but not coupling dark and bright exciton states. Therefore, the interaction between the bright exciton states and the cavity modes is considered in our work, which constitutes a V -type three-level QD structure involving the two neutral exciton transitions (referred to as a V -level QD). A detailed discussion of the dark exciton states, where the magnetic field is in a Voigt configuration, was presented in Ref. [85].

More specifically, as shown in Fig. 2(a), the exciton spin state $|\sigma_+\rangle$ is the bright exciton state with $J_z = +1$, which has right circular polarization. Similarly, the exciton spin state $|\sigma_-\rangle$ is the bright exciton state with $J_z = -1$, which has left circular polarization, and $|G\rangle$ is the neutral ground state with zero energy. The degeneracy of the two exciton spin states is lifted by the anisotropic confinement potential of the QD and its zinc-blende crystal structure, resulting in the fine-structure exchange interaction. Obviously, the exciton spin states $|\sigma_+\rangle$ and $|\sigma_-\rangle$ are not the eigenstates of the QD system in the anisotropic neutral excitons; therefore we need to introduce the two linearly polarized exciton states $|X\rangle = (|\sigma_+\rangle + |\sigma_-\rangle)/\sqrt{2}$ and $|Y\rangle = i(|\sigma_+\rangle - |\sigma_-\rangle)/\sqrt{2}$, which are the eigenstates of the QD without an external magnetic field [86] and are split between these linearly polarized excitons, known as a fine-structure splitting (denoted by Δ_{FSS}). Since the transitions $|X\rangle \Leftrightarrow |G\rangle$ and $|Y\rangle \Leftrightarrow |G\rangle$ can be optically addressed with the corresponding X -polarized and Y -polarized light, respectively, the states $|X\rangle$ and $|Y\rangle$ are called the linearly X -polarized and the Y -polarized exciton states. Here X and Y are the eigenaxes of the QD. The interaction between the exciton spin states and the bimodal cavity can be transformed into the interaction between the linearly polarized exciton states and the linearly polarized cavity modes [87]. The specific procedures are as follows.

First, in the basis of the two σ exciton spin states $|\sigma_+\rangle$ and $|\sigma_-\rangle$, the QD Hamiltonian can be written as (assuming $\hbar = 1$ hereafter) [73]

$$H_{\text{QD}} = \omega(|\sigma_+\rangle\langle\sigma_+| + |\sigma_-\rangle\langle\sigma_-|) + \frac{\Delta_{FSS}}{2}(|\sigma_+\rangle\langle\sigma_-| + |\sigma_-\rangle\langle\sigma_+|), \quad (1)$$

where the energy of the ground state $|G\rangle$ is set as zero for the sake of simplicity. In addition, $|j\rangle\langle k|$ is the dipole raising

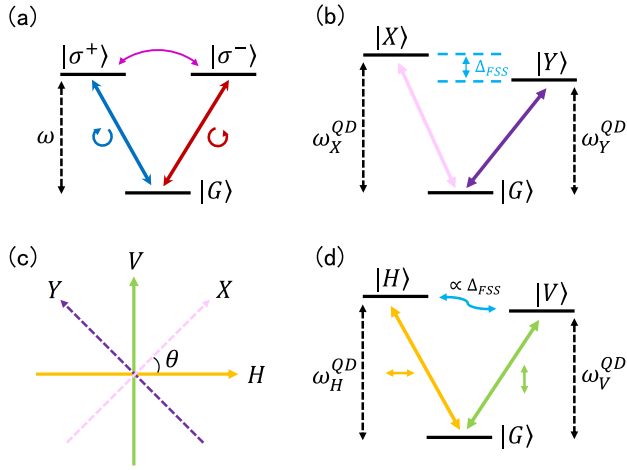


FIG. 2. Energy-level and polarized transition schematic of the ground-state and lowest-energy excited states for the neutral QD inserted in the micropillar cavity (see Fig. 1). (a) The degenerate exciton spin states $|\sigma_+\rangle$ and $|\sigma_-\rangle$ have right and left circular polarizations, $|G\rangle$ is the neutral ground state with zero energy, i.e., the empty QD state, and ω is the transition frequency from the QD exciton spin state to the ground state $|\sigma_+\rangle \Leftrightarrow |G\rangle$ ($|\sigma_-\rangle \Leftrightarrow |G\rangle$). The fine-structure exchange coupling between the exciton spin states $|\sigma_+\rangle$ and $|\sigma_-\rangle$ is represented by the purple solid line, showing that the cylindrical symmetry of the QD is broken in general. (b) The nondegenerate linearly polarized exciton states $|X\rangle$ and $|Y\rangle$ have the corresponding X polarization and Y polarization characteristics induced by the fine-structure exchange interaction. Here ω_X^{QD} (ω_Y^{QD}) is the transition frequency from the QD exciton state to the ground state $|X\rangle \Leftrightarrow |G\rangle$ ($|Y\rangle \Leftrightarrow |G\rangle$) and Δ_{FSS} represents the exciton fine-structure splitting between the two linearly polarized exciton states $|X\rangle$ and $|Y\rangle$. (c) Relative orientation of the cavity and QD eigenaxes. Here θ is the relative angle between the H -polarized cavity mode and the X QD transition. (d) Transformed linearly polarized QD exciton states. Here $|H\rangle$ and $|V\rangle$ are the two orthogonally and linearly polarized exciton states: a horizontal polarization state $|H\rangle$ and a vertical polarization state $|V\rangle$. In addition, ω_H^{QD} (ω_V^{QD}) is the transition frequency between the QD exciton state and the ground state $|H\rangle \Leftrightarrow |G\rangle$ ($|V\rangle \Leftrightarrow |G\rangle$). The coupling between $|H\rangle$ and $|V\rangle$ is proportional to the fine-structure splitting of excitons Δ_{FSS} .

or lowering transition operator between the QD exciton states $|j\rangle$ and $|k\rangle$ (here $j, k = \sigma_-, \sigma_+$ and in the following $j, k = G, X, Y, H, V$), while $|j\rangle\langle j|$ represents the dipole population operator of the QD exciton. The σ exciton spin states with left circular polarization and right circular polarization have degenerate energy ω ; the exchange interaction in the asymmetric QD mixes these two states with the coupling strength $\Delta_{FSS}/2$. It should be noted that the states with double occupation are ignored since we use a low-power laser excitation.

When we take into account the QD Hamiltonian in the basis of the two linearly polarized exciton states $|X\rangle$ and $|Y\rangle$, Eq. (1) can be converted to the form

$$H_{\text{QD}} = \omega_X^{\text{QD}}|X\rangle\langle X| + \omega_Y^{\text{QD}}|Y\rangle\langle Y|. \quad (2)$$

Here the degeneracy of the excitons is lifted owing to the imperfect QD circular symmetry, as shown in Fig. 2(b), and the frequencies of the two linearly polarized excitons are

$\omega_X^{\text{QD}} = \omega + \Delta_{FSS}/2$ with the X polarization and $\omega_Y^{\text{QD}} = \omega - \Delta_{FSS}/2$ with the Y polarization.

Second, in the presence of an external magnetic field B in the Faraday configuration, the magnetic-field-dependent Hamiltonian for the Zeeman interaction of the electron and hole spins can be written in the basis of the two σ exciton spin states $|\sigma_+\rangle$ and $|\sigma_-\rangle$ as [73]

$$H_{\text{mag}} = \beta(|\sigma_+\rangle\langle\sigma_+| - |\sigma_-\rangle\langle\sigma_-|) + \alpha B^2(|\sigma_+\rangle\langle\sigma_+| + |\sigma_-\rangle\langle\sigma_-|), \quad (3)$$

where $\beta = \mu_B B(g_{e,z} + g_{h,z})/2$, with $\mu_B = 57.9 \mu\text{eV/T}$ the Bohr magneton and $g_{e,z} = -0.8$ and $g_{h,z} = -2.2$ the electron and hole effective Landé factors, respectively, in the growth direction (z) according to Refs. [73,85]. The spin splitting of the exciton spin states caused by the Zeeman effect increases linearly with the increase of the magnetic field B . The last term stands for the diamagnetic shift [69] and $\alpha = 20 \mu\text{eV/T}^2$ is the diamagnetic shift coefficient [88].

We consider that in the basis of two linearly polarized exciton states $|X\rangle$ and $|Y\rangle$ the magnetic field applied in the growth direction will mix the two exciton states and lead to diamagnetic shifts. After some calculation, the magnetic-field-dependent Hamiltonian can be transformed into the form

$$H_{\text{mag}} = i\beta(|X\rangle\langle Y| - |Y\rangle\langle X|) + \alpha B^2(|X\rangle\langle X| + |Y\rangle\langle Y|). \quad (4)$$

Third, we focus primarily on the interaction between the three-level QD and the bimodal micropillar cavity. It should be noted that the micropillar cavity considered here has a pair of quasiresonant modes with H and V polarization, respectively. In general, the eigenaxes H and V of the bimodal micropillar cavity differ from the eigenaxes X and Y of the QD by an angle θ , as shown in Fig. 2(c). In order to describe this coupled QD-cavity system more intuitively, we thus replace the exciton eigenstates $|X\rangle$ and $|Y\rangle$ with the orthogonally polarized exciton states $|H\rangle$ and $|V\rangle$ by the transformations [76–78,89]

$$|H\rangle = \cos\theta|X\rangle - \sin\theta|Y\rangle, \quad (5)$$

$$|V\rangle = \sin\theta|X\rangle + \cos\theta|Y\rangle. \quad (6)$$

In order to explicitly express the physical quantities ω_H^{QD} and ω_V^{QD} that represent the transition frequencies between $|H\rangle \Leftrightarrow |G\rangle$ and $|V\rangle \Leftrightarrow |G\rangle$ as shown in Fig. 2(d), based on the above-mentioned transformations (5) and (6), the useful relationships can be derived as

$$\omega_H^{\text{QD}} = \omega_X^{\text{QD}} \cos^2\theta + \omega_Y^{\text{QD}} \sin^2\theta, \quad (7)$$

$$\omega_V^{\text{QD}} = \omega_X^{\text{QD}} \sin^2\theta + \omega_Y^{\text{QD}} \cos^2\theta. \quad (8)$$

Making good use of Eqs. (5) and (6) again, we can acquire the relationships $|X\rangle = \cos\theta|H\rangle + \sin\theta|V\rangle$ and $|Y\rangle = \cos\theta|V\rangle - \sin\theta|H\rangle$. Substituting them into Eqs. (2) and (4), both the QD and magnetic-field-dependent Hamiltonians can be reexpressed in terms of the new orthogonally and linearly

polarized exciton states $|H\rangle$ and $|V\rangle$ as

$$H_{\text{QD}} = \omega_H^{\text{QD}} |H\rangle\langle H| + \omega_V^{\text{QD}} |V\rangle\langle V| + \Delta_{FSS} \sin \theta \cos \theta (|H\rangle\langle V| + |V\rangle\langle H|), \quad (9)$$

$$H_{\text{mag}} = i\beta(|H\rangle\langle V| - |V\rangle\langle H|) + \alpha B^2(|H\rangle\langle H| + |V\rangle\langle V|). \quad (10)$$

Next, under the above transformations, the polarization direction of the new linearly polarized exciton states $|H\rangle$ and $|V\rangle$ are consistent with that of the H - and V -cavity polarization axes and therefore can be optically coupled with the H -polarized and V -polarized cavity modes according to the selection rules [90]. To this end, in the basis of the new linearly polarized exciton states $|H\rangle$ and $|V\rangle$, the cavity-QD interaction Hamiltonian can be written within the rotating-wave and electric dipole approximations as [78]

$$H_{\text{cav}} = \omega_H^{\text{cav}} a_H^\dagger a_H + g_H(|G\rangle\langle H| a_H^\dagger + |H\rangle\langle G| a_H) + \omega_V^{\text{cav}} a_V^\dagger a_V + g_V(|G\rangle\langle V| a_V^\dagger + |V\rangle\langle G| a_V). \quad (11)$$

In the above Hamiltonian (11), the first term is the energy of the unperturbed H -polarized cavity mode. In addition, ω_j^{cav} and a_j^\dagger (a_j) are the cavity resonance frequency and the photon creation (annihilation) operator for the j -polarized cavity mode ($j = H, V$), respectively. For clarity, we have omitted the circumflex for the operators. The second term describes the scenario that the H -polarized cavity mode couples the ground state $|G\rangle$ to the horizontal polarization state $|H\rangle$ of the QD exciton with the coupling strength g_H , where the rotating-wave and electric dipole approximations have been made. Here $|j\rangle\langle G|$ ($|G\rangle\langle j|$) is the dipole raising (lowering) flip operator for the QD exciton transition $|G\rangle \Leftrightarrow |j\rangle$ ($|j\rangle \Leftrightarrow |G\rangle$), also called the exciton creation (annihilation) operator. The third term represents the energy of the unperturbed V -polarized cavity mode. For the first and third terms, we have neglected the zero-point energy, which is allowed since it only gives a relative shift and does not affect the dynamics under study. Finally, the fourth term accounts for the situation that the V -polarized cavity mode couples the ground state $|G\rangle$ to the vertical polarization state $|V\rangle$ with the coupling strength g_V under the rotating-wave and electric dipole approximations. In the above derivation of the Hamiltonian operator, the energy of the ground state $|G\rangle$ is set as zero for the sake of simplicity. Technical details of the associated derivation for Eq. (11) can be easily found in Refs. [11,91].

For notational convenience, we define the quantity ω_c as the central frequency in between the two cavity modes, i.e., $\omega_c = (\omega_H^{\text{cav}} + \omega_V^{\text{cav}})/2$, and the quantity Δ_c as the mode splitting frequency of the bimodal micropillar cavity, i.e., $\Delta_c = \omega_H^{\text{cav}} - \omega_V^{\text{cav}}$. The cavity resonance frequencies of the H - and V -polarized cavity modes can be expressed as $\omega_H^{\text{cav}} = \omega_c + \Delta_c/2$ and $\omega_V^{\text{cav}} = \omega_c - \Delta_c/2$ [84,87], respectively. On the other hand, the linearly polarized exciton states $|H\rangle$ and $|V\rangle$ are coupled to the cavity modes a_H and a_V with the same polarization and the coupling strengths are g_H and g_V , respectively. Here we take into account the case that $g_H = g_V = g$, which means the coupling strengths between the cavity modes and the exciton transitions are independent of the polarization [78].

Along the lines of Ref. [79], the cavity is pumped by an input cw laser field along the H -polarized cavity mode axis. In this case, the pump-field-dependent Hamiltonian can be expressed as

$$H_{\text{pump}} = \Omega(a_H e^{i\omega_L t} + a_H^\dagger e^{-i\omega_L t}), \quad (12)$$

where Ω and ω_L are the strength and frequency of the pump laser field, respectively.

Finally, the total Hamiltonian of our CQED system includes four items [see Eqs. (9)–(12)] discussed above, i.e.,

$$H_{\text{tot}} = H_{\text{QD}} + H_{\text{mag}} + H_{\text{cav}} + H_{\text{pump}}. \quad (13)$$

In a frame rotating at the frequency ω_L of the pump laser field, the resulting Hamiltonian of the whole CQED system in the basis of the two linearly polarized exciton states $|H\rangle$ and $|V\rangle$ can be explicitly written as

$$\begin{aligned} H_{\text{tot}} = & \delta_H^{\text{QD}} |H\rangle\langle H| + \delta_V^{\text{QD}} |V\rangle\langle V| \\ & + \Delta_{FSS} \sin \theta \cos \theta (|H\rangle\langle V| + |V\rangle\langle H|) \\ & + i\beta(|H\rangle\langle V| - |V\rangle\langle H|) + \alpha B^2(|H\rangle\langle H| + |V\rangle\langle V|) \\ & + \left(\Delta_{CL} + \frac{\Delta_c}{2} \right) a_H^\dagger a_H + g(|G\rangle\langle H| a_H^\dagger + |H\rangle\langle G| a_H) \\ & + \left(\Delta_{CL} - \frac{\Delta_c}{2} \right) a_V^\dagger a_V + g(|G\rangle\langle V| a_V^\dagger + |V\rangle\langle G| a_V) \\ & + \Omega(a_H + a_H^\dagger), \end{aligned} \quad (14)$$

with

$$\delta_H^{\text{QD}} = \delta_X^{\text{QD}} \cos^2 \theta + \delta_Y^{\text{QD}} \sin^2 \theta, \quad (15)$$

$$\delta_V^{\text{QD}} = \delta_X^{\text{QD}} \sin^2 \theta + \delta_Y^{\text{QD}} \cos^2 \theta, \quad (16)$$

where $\delta_X^{\text{QD}} = \omega_X^{\text{QD}} - \omega_L = \Delta_{CL} + \delta + \Delta_{FSS}/2$ and $\delta_Y^{\text{QD}} = \omega_Y^{\text{QD}} - \omega_L = \Delta_{CL} + \delta - \Delta_{FSS}/2$ are the detunings of the two exciton transition frequencies ω_X^{QD} and ω_Y^{QD} from the frequency ω_L of the external pump laser field, respectively. Also, $\Delta_{CL} = \omega_c - \omega_L$ is the detuning between the central frequency ω_c [$\omega_c \equiv (\omega_H^{\text{cav}} + \omega_V^{\text{cav}})/2$] of the micropillar cavity modes and the frequency ω_L of the external pump laser field. In addition, $\delta = \omega - \omega_c$ is the center detuning between the central frequency ω [$\omega \equiv (\omega_H^{\text{QD}} + \omega_V^{\text{QD}})/2 = (\omega_X^{\text{QD}} + \omega_Y^{\text{QD}})/2$] of the linearly polarized excitons and the central frequency ω_c of the micropillar cavity modes. It should be noted that the third and fourth terms on the right-hand side of Eq. (14) are the coupling terms, which manipulate the oscillation rate between the two exciton states $|H\rangle$ and $|V\rangle$ and thus affect the generation of the V -polarized photons. Evidently, the third term on the right-hand side of Eq. (14) is closely related to the fine-structure splitting Δ_{FSS} and the direction angle θ , and the fourth term is associated with the external magnetic field B , whose role is detailed afterward. Under the special conditions that both there is no external magnetic field, e.g., $B = 0$, and the eigenaxes of the excitons coincide with the eigenaxes of the cavity modes, e.g., $\theta = 0$ or $\theta = \pi/2$, there will be no V -polarized photons generated in the cavity.

B. Lindblad master equation governing the dissipative dynamics

To solve incoherent processes and study the dynamics of the CQED system with density matrix operator ρ , we utilize the Lindblad master equation [11,91]

$$\begin{aligned} \frac{d\rho}{dt} = & -i[H_{\text{tot}}, \rho] + L_H^{\text{cav}}[\rho] + L_V^{\text{cav}}[\rho] \\ & + L_H^{\text{sp}}[\rho] + L_V^{\text{sp}}[\rho] + L^{\text{deph}}[\rho]. \end{aligned} \quad (17)$$

Here the superoperator of our system is in the form $L[\rho] = A\rho A^\dagger - AA^\dagger\rho/2 - \rho A^\dagger A/2$, where A is a collapse operator describing the dissipative processes. To be specific, the second and third terms represent the decays of the two linearly polarized cavity modes, and the cavity dampings associated with the cavity optical losses are described by the collapse operators $A_H^{\text{cav}} = \sqrt{\kappa_H}a_H$ and $A_V^{\text{cav}} = \sqrt{\kappa_V}a_V$. Here κ_H and κ_V are the cavity decay rates of the H -polarized and V -polarized cavity modes, respectively. The fourth and fifth terms represent the spontaneous emission processes of a photon into the external environment and are described by the collapse operators $A_H^{\text{QD}} = \sqrt{\gamma_H^{\text{sp}}}|G\rangle\langle H|$ and $A_V^{\text{QD}} = \sqrt{\gamma_V^{\text{sp}}}|G\rangle\langle V|$, where γ_H^{sp} and γ_V^{sp} are the spontaneous emission rates of the three-level QD. The last term represents the exciton pure dephasing associated with the QD decoherence processes, which are described by the collapse operators $A_H^{\text{dp}} = \sqrt{2\gamma_H^{\text{dp}}}|H\rangle\langle H|$ and $A_V^{\text{dp}} = \sqrt{2\gamma_V^{\text{dp}}}|V\rangle\langle V|$, where γ_H^{dp} and γ_V^{dp} are the exciton pure dephasing rates. We can numerically solve Eq. (17) by expressing the operators on an occupation number Fock basis, truncated to the most suitable photon number previously checked for convergence.

C. Second-order intensity correlation function providing information on photon (anti)bunching

In order to better describe the statistical properties of the photons in the cavity, the equal-time second-order intensity correlation function is introduced, with the form

$$g_O^{(2)}(0) = \frac{\text{Tr}(\rho_{\text{ss}} O^\dagger O^\dagger O O)}{[\text{Tr}(\rho_{\text{ss}} O^\dagger O)]^2}, \quad (18)$$

where ρ_{ss} is the steady-state solution corresponding to $d\rho/dt = 0$ in Eq. (17). The symbol O denotes the photon annihilation operator for the cavity mode with H polarization, i.e., $O = a_H$, or for the cavity mode with V polarization, i.e., $O = a_V$.

The equal-time second-order intensity correlation function $g_O^{(2)}(0)$ can be used as an important index to evaluate the statistical properties of the photons. More specifically, a value of $g_O^{(2)}(0) > 1$ corresponds to the photon bunching effect; in other words, photons are in a super-Poisson distribution, which is a classical effect. A value of $g_O^{(2)}(0) = 1$ corresponds to the coherent-state photons that are in a Poissonian distribution, which is a quasiclassical effect. A value of $g_O^{(2)}(0) < 1$ corresponds to the photon antibunching effect; in other words, photons are in a sub-Poisson distribution, which is a quantum effect. The smaller the value of $g_O^{(2)}(0)$ is, the better the quantum properties of photons are. A value of $g_O^{(2)}(0) \rightarrow 0$

suggests that the system can be used to produce the complete photon blockade phenomenon [92], which is a candidate for an ideal single-photon source. The single-photon regime is usually characterized by $g_O^{(2)}(0) < 0.5$. Finally, it should be pointed out that in the following discussion the input pump laser field is set such that the H -polarized cavity mode is excited but the photons emitted from the V -polarized cavity mode are detected, i.e., in a cross-polarized detection scheme like Ref. [79]. For a detailed description of this V -level QD–micropillar cavity system, we refer the reader to Refs. [76–81].

III. APPROXIMATE SOLUTIONS OF THE SECOND-ORDER CORRELATION FUNCTION VIA THE SCHRÖDINGER EQUATION APPROACH UNDER THE WEAK-PUMP CONDITION

Before proceeding, we want to supply an approximately analytical expression for the equal-time second-order intensity correlation function as an alternative method to characterize the photon statistical properties of the present CQED system [82,83]. Adopting the techniques introduced in Refs. [42,43,45], in the weak-pump limit ($\Omega \ll \kappa_H$ and κ_V), the time-dependent state of the system is well approximated in the two-excitation manifold as

$$\begin{aligned} |\Psi(t)\rangle = & C_{00G}|0, 0, G\rangle + C_{10G}|1, 0, G\rangle + C_{01G}|0, 1, G\rangle \\ & + C_{00H}|0, 0, H\rangle + C_{00V}|0, 0, V\rangle + C_{20G}|2, 0, G\rangle \\ & + C_{02G}|0, 2, G\rangle + C_{11G}|1, 1, G\rangle + C_{10H}|1, 0, H\rangle \\ & + C_{10V}|1, 0, V\rangle + C_{01H}|0, 1, H\rangle + C_{01V}|0, 1, V\rangle. \end{aligned} \quad (19)$$

Here $|m, n, j\rangle = |m\rangle \otimes |n\rangle \otimes |j\rangle$ defines a state with m photons in the H -polarized cavity mode, n photons in the V -polarized cavity mode, and the QD exciton in the state of $|j\rangle$ ($j = G, H, V$). The coefficient C_{mnj} stands for the probability amplitude of the corresponding state $|m, n, j\rangle$. Taking into account the decays of the two cavity modes and the dampings of the QD excitons, the dynamical evolution of the above coefficients C_{mnj} can be derived from the solution of the Schrödinger equation $i\partial|\Psi(t)\rangle/\partial t = \tilde{H}|\Psi(t)\rangle$, written for the non-Hermitian Hamiltonian

$$\begin{aligned} \tilde{H} = & H_{\text{tot}} - i\frac{\kappa_H}{2}a_H^\dagger a_H - i\frac{\kappa_V}{2}a_V^\dagger a_V \\ & - i\frac{\gamma_H^{\text{sp}}}{2}|G\rangle\langle H| - i\frac{\gamma_V^{\text{sp}}}{2}|G\rangle\langle V| \\ & - i\gamma_H^{\text{dp}}|H\rangle\langle H| - i\gamma_V^{\text{dp}}|V\rangle\langle V|, \end{aligned} \quad (20)$$

with H_{tot} given in Eq. (14).

Inserting the wave function [Eq. (19)] and Hamiltonian [Eq. (20)] into the Schrödinger equation, the coefficients C_{mnj} satisfy the equations of motion

$$\begin{aligned} i\frac{\partial C_{10G}}{\partial t} = & \left(\Delta_{CL} + \frac{\Delta_c}{2} - i\frac{\kappa_H}{2}\right)C_{10G} + gC_{00H} \\ & + \sqrt{2}\Omega C_{20G} - i\frac{\gamma_H^{\text{sp}}}{2}C_{10H} - i\frac{\gamma_V^{\text{sp}}}{2}C_{10V} \\ & + \Omega C_{00G}, \end{aligned} \quad (21)$$

$$i\frac{\partial C_{01G}}{\partial t} = \left(\Delta_{CL} - \frac{\Delta_c}{2} - i\frac{\kappa_V}{2}\right)C_{01G} + gC_{00V} - i\frac{\gamma_H^{sp}}{2}C_{01H} - i\frac{\gamma_V^{sp}}{2}C_{01V} + \Omega C_{11G}, \quad (22)$$

$$i\frac{\partial C_{00H}}{\partial t} = (\Delta_{FSS} \sin \theta \cos \theta + i\beta)C_{00V} + \Omega C_{10H} + gC_{10G} + (\delta_H^{QD} + \alpha B^2 - i\gamma_H^{dp})C_{00H}, \quad (23)$$

$$i\frac{\partial C_{00V}}{\partial t} = (\Delta_{FSS} \sin \theta \cos \theta - i\beta)C_{00H} + \Omega C_{10V} + gC_{01G} + (\delta_V^{QD} + \alpha B^2 - i\gamma_V^{dp})C_{00V}, \quad (24)$$

$$i\frac{\partial C_{20G}}{\partial t} = \sqrt{2}\Omega C_{10G} + 2\left(\Delta_{CL} + \frac{\Delta_c}{2} - i\frac{\kappa_H}{2}\right)C_{20G} + \sqrt{2}gC_{10H}, \quad (25)$$

$$i\frac{\partial C_{02G}}{\partial t} = 2\left(\Delta_{CL} - \frac{\Delta_c}{2} - i\frac{\kappa_V}{2}\right)C_{02G} + \sqrt{2}gC_{01V}, \quad (26)$$

$$i\frac{\partial C_{11G}}{\partial t} = \left(\Delta_{CL} + \frac{\Delta_c}{2} - i\frac{\kappa_H}{2}\right)C_{11G} + \Omega C_{01G} + \left(\Delta_{CL} - \frac{\Delta_c}{2} - i\frac{\kappa_V}{2}\right)C_{11G} + gC_{01H} + gC_{10V}, \quad (27)$$

$$i\frac{\partial C_{10H}}{\partial t} = (\Delta_{FSS} \sin \theta \cos \theta + i\beta)C_{10V} + \sqrt{2}gC_{20G} + (\delta_H^{QD} + \alpha B^2 - i\gamma_H^{dp})C_{10H} + \Omega C_{00H} + \left(\Delta_{CL} + \frac{\Delta_c}{2} - i\frac{\kappa_H}{2}\right)C_{10H}, \quad (28)$$

$$i\frac{\partial C_{10V}}{\partial t} = (\Delta_{FSS} \sin \theta \cos \theta - i\beta)C_{10H} + gC_{11G} + (\delta_V^{QD} + \alpha B^2 - i\gamma_V^{dp})C_{10V} + \Omega C_{00V} + \left(\Delta_{CL} + \frac{\Delta_c}{2} - i\frac{\kappa_H}{2}\right)C_{10V}, \quad (29)$$

$$i\frac{\partial C_{01H}}{\partial t} = (\delta_H^{QD} + \alpha B^2 - i\gamma_H^{dp})C_{01H} + gC_{11G} + (\Delta_{FSS} \sin \theta \cos \theta + i\beta)C_{01V} + \left(\Delta_{CL} - \frac{\Delta_c}{2} - i\frac{\kappa_V}{2}\right)C_{01H}, \quad (30)$$

$$i\frac{\partial C_{01V}}{\partial t} = (\delta_V^{QD} + \alpha B^2 - i\gamma_V^{dp})C_{01V} + \sqrt{2}gC_{02G} + (\Delta_{FSS} \sin \theta \cos \theta - i\beta)C_{01H} + \left(\Delta_{CL} - \frac{\Delta_c}{2} - i\frac{\kappa_V}{2}\right)C_{01V}. \quad (31)$$

In the steady state $\partial C_{mnj}/\partial t = 0$, the equations for the coefficients C_{mnj} are given as

$$0 = \left(\Delta_{CL} + \frac{\Delta_c}{2} - i\frac{\kappa_H}{2}\right)C_{10G} + gC_{00H} + \sqrt{2}\Omega C_{20G} - i\frac{\gamma_H^{sp}}{2}C_{10H} - i\frac{\gamma_V^{sp}}{2}C_{10V} + \Omega C_{00G}, \quad (32)$$

$$0 = \left(\Delta_{CL} - \frac{\Delta_c}{2} - i\frac{\kappa_V}{2}\right)C_{01G} + gC_{00V} - i\frac{\gamma_H^{sp}}{2}C_{01H} - i\frac{\gamma_V^{sp}}{2}C_{01V} + \Omega C_{11G}, \quad (33)$$

$$0 = (\Delta_{FSS} \sin \theta \cos \theta + i\beta)C_{00V} + \Omega C_{10H} + gC_{10G} + (\delta_H^{QD} + \alpha B^2 - i\gamma_H^{dp})C_{00H}, \quad (34)$$

$$0 = (\Delta_{FSS} \sin \theta \cos \theta - i\beta)C_{00H} + \Omega C_{10V} + gC_{01G} + (\delta_V^{QD} + \alpha B^2 - i\gamma_V^{dp})C_{00V}, \quad (35)$$

$$0 = \sqrt{2}\Omega C_{10G} + 2\left(\Delta_{CL} + \frac{\Delta_c}{2} - i\frac{\kappa_H}{2}\right)C_{20G} + \sqrt{2}gC_{10H}, \quad (36)$$

$$0 = 2\left(\Delta_{CL} - \frac{\Delta_c}{2} - i\frac{\kappa_V}{2}\right)C_{02G} + \sqrt{2}gC_{01V}, \quad (37)$$

$$0 = \left(\Delta_{CL} + \frac{\Delta_c}{2} - i\frac{\kappa_H}{2}\right)C_{11G} + \Omega C_{01G} + \left(\Delta_{CL} - \frac{\Delta_c}{2} - i\frac{\kappa_V}{2}\right)C_{11G} + gC_{01H} + gC_{10V}, \quad (38)$$

$$0 = (\Delta_{FSS} \sin \theta \cos \theta + i\beta)C_{10V} + \sqrt{2}gC_{20G} + (\delta_H^{QD} + \alpha B^2 - i\gamma_H^{dp})C_{10H} + \Omega C_{00H} + \left(\Delta_{CL} + \frac{\Delta_c}{2} - i\frac{\kappa_H}{2}\right)C_{10H}, \quad (39)$$

$$0 = (\Delta_{FSS} \sin \theta \cos \theta - i\beta)C_{10H} + gC_{11G} + (\delta_V^{QD} + \alpha B^2 - i\gamma_V^{dp})C_{10V} + \Omega C_{00V} + \left(\Delta_{CL} + \frac{\Delta_c}{2} - i\frac{\kappa_H}{2}\right)C_{10V}, \quad (40)$$

$$0 = (\delta_H^{QD} + \alpha B^2 - i\gamma_H^{dp})C_{01H} + gC_{11G} + (\Delta_{FSS} \sin \theta \cos \theta + i\beta)C_{01V} + \left(\Delta_{CL} - \frac{\Delta_c}{2} - i\frac{\kappa_V}{2}\right)C_{01H}, \quad (41)$$

$$0 = (\delta_V^{QD} + \alpha B^2 - i\gamma_V^{dp})C_{01V} + \sqrt{2}gC_{02G} + (\Delta_{FSS} \sin \theta \cos \theta - i\beta)C_{01H} + \left(\Delta_{CL} - \frac{\Delta_c}{2} - i\frac{\kappa_V}{2}\right)C_{01V}. \quad (42)$$

According to Eqs. (32)–(42), we can outline the energy levels showing the zero-, one-, and two-photon states (horizontal gray lines without arrows) and the excitation pathways (colored lines with arrows) in the two-photon manifold, as displayed in Fig. 3. Remarkably, the quantum interference can happen between different two-photon excitation pathways due mainly to the unique V -level configuration of the QD exciton. This is equivalent to the cavity-coupling-cavity induced quantum interference, as in Refs. [42,43,45,49,51]. As a final remark we point out that the physics behind the photon

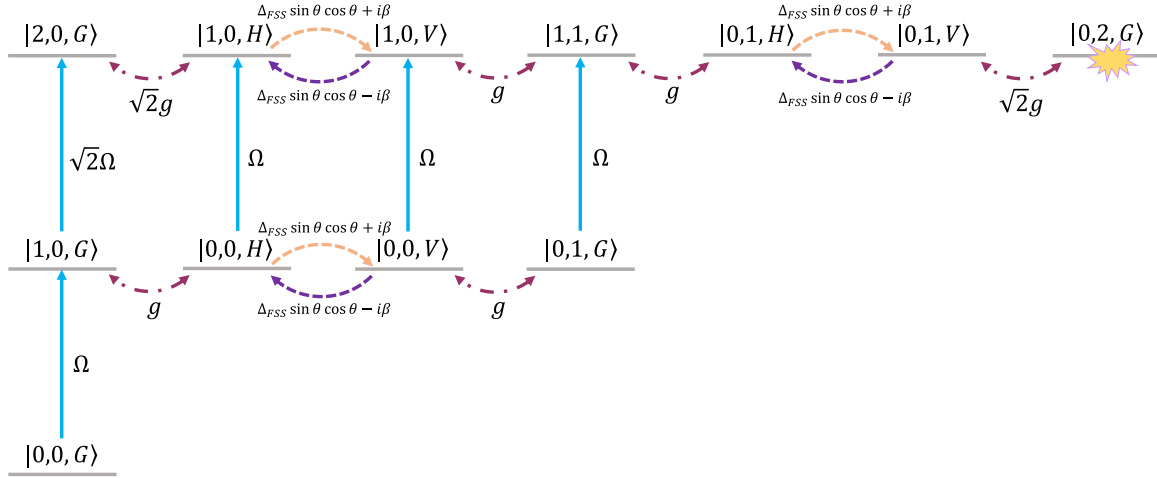


FIG. 3. Energy-level diagram in the two-photon manifold and the corresponding transition pathways. States are labeled by $|m, n, j\rangle$ with the first number representing the Fock state for the H -polarized cavity mode with the photon number m , the second number representing the Fock state for the V -polarized cavity mode with the photon number n , and the third number being the exciton state of the QD.

statistical properties is the effect of quantum interference between different excitation pathways.

Alternatively, under the weak-pump condition, we have the relationship

$$\begin{aligned} C_{00G} &\gg \{C_{10G}, C_{01G}, C_{00H}, C_{00V}\} \\ &\gg \{C_{20G}, C_{02G}, C_{11G}, C_{10H}, C_{10V}, C_{01H}, C_{01V}\} \\ &\gg \dots \end{aligned} \quad (43)$$

In this circumstance given by Eq. (43), by utilizing the formula $a_V^\dagger a_V |m, n, j\rangle = n |m, n, j\rangle$ for the V polarization and the expression of the wave function $|\Psi(t)\rangle$ from Eq. (19), the average number of photons n_V with the V polarization and the normalized zero-time-delay second-order correlation function $g_V^{(2)}(0)$ can thus be expressed in terms of the coefficients C_{mnj} as [49,51]

$$\begin{aligned} A &= \langle a_V^\dagger a_V^\dagger a_V a_V \rangle = \langle (a_V^\dagger a_V)^2 \rangle - \langle a_V^\dagger a_V \rangle^2 \\ &= \sum_{m,n,j} n(n-1) |C_{mnj}|^2 = 2|C_{02G}|^2 + \dots \simeq 2|C_{02G}|^2, \end{aligned} \quad (44)$$

$$\begin{aligned} N_V &= \langle a_V^\dagger a_V \rangle = \sum_{m,n,j} n |C_{mnj}|^2 \\ &= |C_{01G}|^2 + |C_{01H}|^2 + |C_{01V}|^2 + |C_{11G}|^2 \\ &\quad + 2|C_{02G}|^2 + \dots \simeq |C_{01G}|^2, \end{aligned} \quad (45)$$

$$g_V^{(2)}(0) = \frac{\langle a_V^\dagger a_V^\dagger a_V a_V \rangle}{(\langle a_V^\dagger a_V \rangle)^2} = \frac{A}{N_V^2} \simeq \frac{2|C_{02G}|^2}{|C_{01G}|^4}, \quad (46)$$

with the sum indices m, n, j being $m, n = 0, 1, 2, \dots$ and $j = G, H, V$ in the expressions (44) and (45) and with the

abbreviation $\langle \bullet \rangle$ denoting $\langle \bullet \rangle \equiv \langle \Psi(t) | \bullet | \Psi(t) \rangle$, where $|\Psi(t)\rangle$ is yielded by Eq. (19).

It is obvious that the above coupled algebraic equations (32)–(42) are closed, i.e., 11 equations for 11 unknown coefficients. As a result, from a mathematical point of view, a complete solution for the coefficients C_{mnj} and further for the second-order correlation function $g_V^{(2)}(0)$ is attainable by directly solving the above coupled algebraic equations (32)–(42). Unfortunately, the expression of the analytical solution is very lengthy and it is very difficult to see the physics (not shown). The analytical solution obtained here is validated by the numerical calculation based on the master equation. From the detailed derivation processes and Fig. 3 it turns out that the second-order correlation function $g_V^{(2)}(0)$ is closely related to the coupling strength between the cavity modes and the exciton transitions g , the applied magnetic field B ($\beta \propto B$), and also the exciton fine-structure splitting Δ_{FFS} . In what follows we are more interested in the influence of the tunable magnetic field and the exciton fine-structure splitting on the photon statistics of the CQED system.

In Fig. 4, the numerical results of the equal-time second-order intensity correlation function $g_V^{(2)}(0)$ given by the master equation are compared with the analytical results given by the Schrödinger equation in the steady state. We plot the equal-time second-order intensity correlation function $g_V^{(2)}(0)$ as a function of the external magnetic field B in Fig. 4(a). The purple solid line corresponds to the numerical solution, while the blue-circle line corresponds to the analytical solution. We also display the equal-time second-order intensity correlation function $g_V^{(2)}(0)$ varying with the QD-cavity coupling strength g in Fig. 4(b). The yellow solid line represents the numerical result and the green-triangle line represents the analytical result. Whether in Fig. 4(a) or 4(b), it is revealed that the results of both the numerical solution and the analytical solution are in good agreement. In other words, the analytical solution obtained by the Schrödinger equation in the steady state can be faithfully reproduced by the full numerical solution obtained by the master equation.

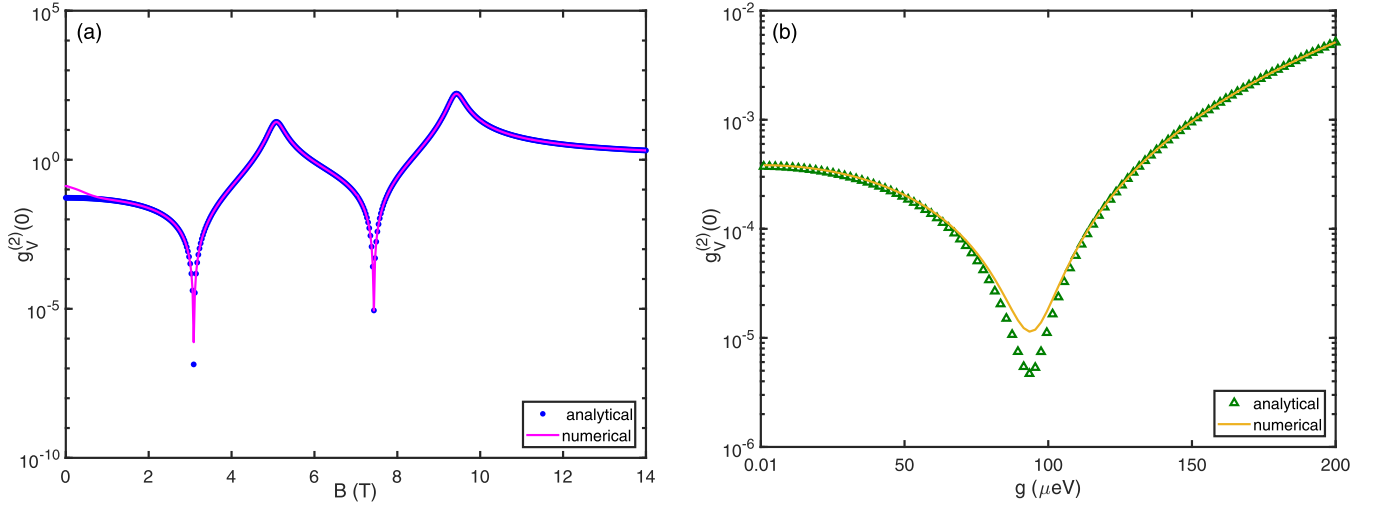


FIG. 4. Comparison between the numerical and analytical results of the equal-time second-order intensity correlation function $g_V^{(2)}(0)$ for the V -polarized photons. (a) Equal-time second-order intensity correlation function $g_V^{(2)}(0)$ varying with the external magnetic field B for both the numerical result (purple solid line) and the analytical result (blue-circle line). The relevant parameters used in this plot are borrowed from recent state-of-the-art experiments [76–78]: $\kappa_H = 100$ μeV , $\kappa_V = 100$ μeV , $\gamma_H^{sp} = 0.6$ μeV , $\gamma_V^{sp} = 0.6$ μeV , $g = 20$ μeV , $\Delta_{FSS} = 10$ μeV , $\Delta_c = 70$ μeV , $\theta = 45^\circ$, $\delta = 0$, and $\Omega = 10$ μeV , respectively. (b) Equal-time second-order intensity correlation function $g_V^{(2)}(0)$ of the V -polarized photons as a function of the QD-cavity coupling strength g for both the numerical result (yellow solid line) and the analytical result (green-triangle line). The system parameters used here are $\kappa_H = 100$ μeV , $\kappa_V = 100$ μeV , $\gamma_H^{sp} = 0.6$ μeV , $\gamma_V^{sp} = 0.6$ μeV , $B = 3$ T, $\Delta_{FSS} = 10$ μeV , $\Delta_c = 70$ μeV , $\theta = 45^\circ$, $\delta = 0$, and $\Omega = 10$ μeV , respectively. Here, the dephasing of the QD has been neglected for convenience of the analytical calculations and, in Sec. IV, it will be included.

IV. NUMERICAL RESULTS ABOUT STEADY-STATE PHOTON OCCUPATION AND CORRELATION

In order to evaluate our proposed scheme, the following experimental parameters of the QD-cavity system are used in the numerical simulations unless noted otherwise: the cavity decay rates of the H -polarized and V -polarized cavity modes $\kappa_H = \kappa_V = \kappa = 100$ μeV , the spontaneous emission rates of the QD excitons $\gamma_H^{sp} = \gamma_V^{sp} = \gamma = 0.6$ μeV , the pure dephasing rates of the QD excitons $\gamma_H^{dp} = 3$ μeV and $\gamma_V^{dp} = 3$ μeV , the exciton fine-structure splitting of the QD $\Delta_{FSS} = 10$ μeV , the mode splitting frequency of the H and V polarizations $\Delta_c = 70$ μeV , the relative orientation of the QD and cavity axes $\theta = 20^\circ$, and the strength of the pump laser field $\Omega = 10$ μeV . Typical values of these experimental parameters are taken from Refs. [76–78]. Detailed results in the steady state are presented in Figs. 5–10 by directly solving the master equation.

Figure 5 shows the equal-time second-order intensity correlation function $g_V^{(2)}(0)$ and the photon occupation (also called the cavity average photon number) $\langle a_V^\dagger a_V \rangle$, with the V polarization as a function of the frequency detuning Δ_{CL} between the center frequency (ω_c) of the micropillar cavity modes and the frequency (ω_L) of the pump laser field under the condition of weak coupling between the QD and the cavity. Here we set the QD-cavity coupling strength $g = 20$ μeV , which is taken from experimental works [76–78] and satisfies the weak-coupling CQED regime. It is clearly shown in the figure that the main peak of the V -polarized photon number appears near the point $\Delta_{CL} = 85$ μeV , where the value of the second-order correlation function is $g_V^{(2)}(0) = 3.6 \times 10^{-3}$. At the same time, the secondary peak of the V -polarized photon

number appears near the point $\Delta_{CL} = -440$ μeV , where the value of the second-order correlation function reaches $g_V^{(2)}(0) = 4.7 \times 10^{-4}$.

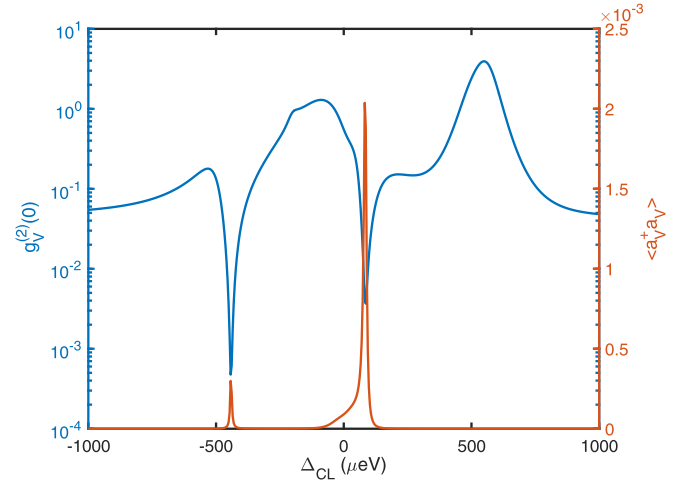


FIG. 5. Equal-time second-order intensity correlation function $g_V^{(2)}(0)$ and photon occupation, i.e., cavity average photon number, $\langle a_V^\dagger a_V \rangle$, with the V polarization in the steady state, varying with the detuning Δ_{CL} between the center frequency ω_c of the cavity modes and the frequency ω_L of the pump laser field. The system parameters used here are $\kappa = 100$ μeV , $\gamma = 0.6$ μeV , $\gamma_H^{dp} = 3$ μeV , $\gamma_V^{dp} = 3$ μeV , $g = 20$ μeV , $B = 3$ T, $\Delta_{FSS} = 10$ μeV , $\Delta_c = 70$ μeV , $\theta = 20^\circ$, $\delta = 0$, and $\Omega = 10$ μeV . The upper curve with two sharp dips corresponds to the left vertical coordinate-axis and the value of $g_V^{(2)}(0)$, while the lower curve with two sharp peaks corresponds to the right vertical coordinate-axis and the value of $\langle a_V^\dagger a_V \rangle$.

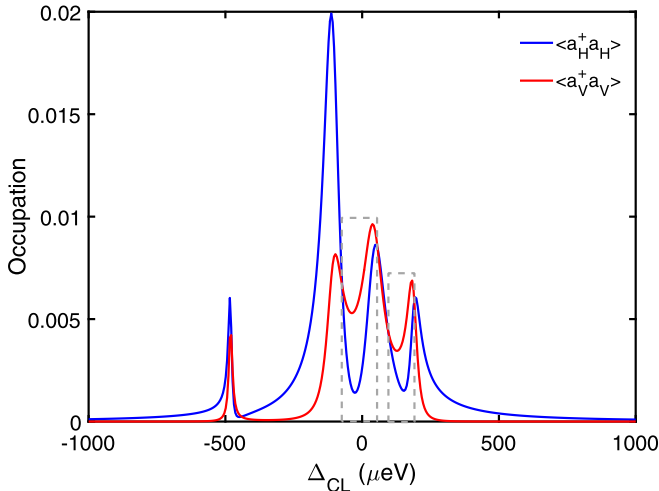


FIG. 6. Photon occupations $\langle a_V^\dagger a_V \rangle$ and $\langle a_H^\dagger a_H \rangle$, with the H and V polarizations in the steady state, as a function of the detuning Δ_{CL} between the center frequency ω_c of the two cavity modes and the frequency ω_L of the pump laser field. The system parameters used here are $\kappa = 100 \mu\text{eV}$, $\gamma = 0.6 \mu\text{eV}$, $\gamma_H^{dp} = 3 \mu\text{eV}$, $\gamma_V^{dp} = 3 \mu\text{eV}$, $g = 140 \mu\text{eV}$, $B = 3 \text{ T}$, $\Delta_{FSS} = 10 \mu\text{eV}$, $\Delta_c = 70 \mu\text{eV}$, $\theta = 20^\circ$, $\delta = 0$, and $\Omega = 10 \mu\text{eV}$. The highest peak curve corresponds to the value of $\langle a_H^\dagger a_H \rangle$, while the other corresponds to the value of $\langle a_V^\dagger a_V \rangle$.

Using the input-output formalism [11], we define the operator $f_V^{(\text{out})}$ describing the V -polarized transmission field and yield the continuity relation $f_V^{(\text{out})} = \sqrt{\kappa^{\text{top}}} a_V$, with κ^{top} the cavity damping rate through the top mirror. In the previous scheme proposed by Zhang *et al.* [93], the photon statistics in the CQED system consisting of a single two-level QD coupled to a two-mode cavity are explored in the absence of the external magnetic field. In that system the region with an equal-time second-order intensity correlation function less than unity corresponds to the dip region of the average photon number, where the average photon number exhibits a peak-dip-peak symmetric structure, that is to say, the photons with strong antibunching but with low transmission are produced [93]. Contrary to Ref. [93], in our system, the phenomenon in which the point of the maximum average photon number corresponds to the point of the minimum of the second-order correlation function $g_V^{(2)}(0)$ implies a meaningful result: It is possible to obtain high transmission photons with a strong antibunching effect in our CQED system under consideration, which is not only useful for related measurements [19], but also meaningful for designing practical experiments. In addition, the photon antibunching effect in a large frequency detuning range makes it possible to prepare more feasible single-photon sources with multiple frequencies, which is different from previous studies [42,43] on the photon blockade only for specific optical detuning, which further increases the possibility of experimental realization.

The occupations of the two linearly polarized cavity modes under strong coupling are plotted in Fig. 6 as a function of the frequency detuning Δ_{CL} between the center frequency (ω_c) of the cavity modes and the center frequency (ω_L) of the pump laser field. The part of the figure that is framed by the dashed-line box emphasizes the fact that the number of V -polarized photons exceeds the number of H -polarized

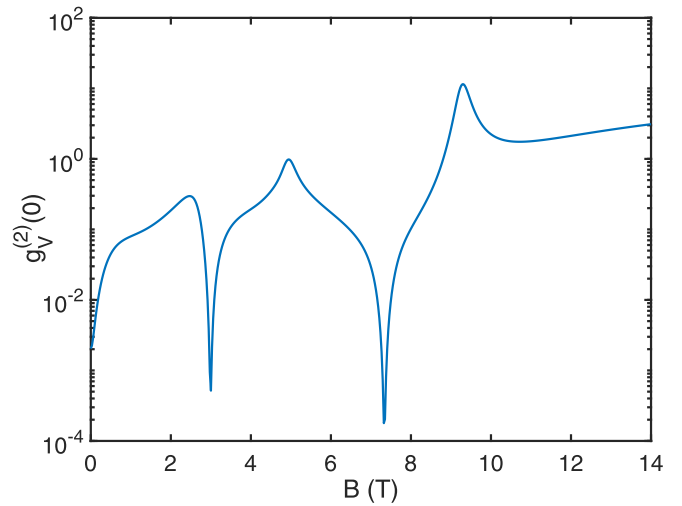


FIG. 7. Semilogarithmic plot of the equal-time second-order intensity correlation function $g_V^{(2)}(0)$ of the V -polarized photons as a function of the external magnetic field B . The other parameters of the CQED system are $\kappa = 100 \mu\text{eV}$, $\gamma = 0.6 \mu\text{eV}$, $\gamma_H^{dp} = 3 \mu\text{eV}$, $\gamma_V^{dp} = 3 \mu\text{eV}$, $g = 20 \mu\text{eV}$, $\Delta_{CL} = -440 \mu\text{eV}$, $\Delta_{FSS} = 10 \mu\text{eV}$, $\Delta_c = 70 \mu\text{eV}$, $\theta = 20^\circ$, $\delta = 0$, and $\Omega = 10 \mu\text{eV}$.

photons under certain detuning. In other words, the cavity mode with the V polarization is more populated, which can be used as a photon polarization switch [88].

This naturally raises the question of what causes the generation of the V -polarized photons. As we discussed in Sec. II A, the physical reason for generating the V -polarized photons in the micropillar cavity is the Rabi oscillation between the QD and the cavity modes under the external driving laser field Ω and the coherent interaction between the exciton states $|H\rangle$ and $|V\rangle$ under the external magnetic field B . More specifically, when an external driving laser field Ω pumps the H -polarized cavity mode, the linearly polarized exciton state with the H polarization $|H\rangle$ is excited due to the coherent coupling between the QD and the cavity. The exciton states $|H\rangle$ and $|V\rangle$ will be mixed because of the existence of the applied magnetic field and the coherent coupling via the terms $i\beta(|H\rangle\langle V| - |V\rangle\langle H|)$ and $\Delta_{FSS} \sin \theta \cos \theta (|H\rangle\langle V| + |V\rangle\langle H|)$ [cf. Eq. (14)], resulting in the interaction between the linearly polarized exciton states. This eventually leads to the indirect excitation of the linearly polarized exciton state with the V polarization and then the emergence of the V -polarized photons in the CQED system.

For the purpose of exploring the influence of the applied magnetic field B on the photon statistical properties of the CQED system, the equal-time second-order intensity correlation function of the V -polarized photons $g_V^{(2)}(0)$ versus the strength of the magnetic field B is plotted in Fig. 7. It is worth emphasizing that only when both the cavity and the QD are weakly coupled do we consider the impact of the magnetic field B on the V -polarized photons. It can be seen more clearly from Fig. 7 that when the strength of the magnetic field is not very large, the statistical properties of the V -polarized photons in the cavity are in the sub-Poisson distribution, that is to say, in the state of photon antibunching. With the increase of the applied magnetic field B , the bunching effect of the V -polarized photons gradually appears. Within the range of

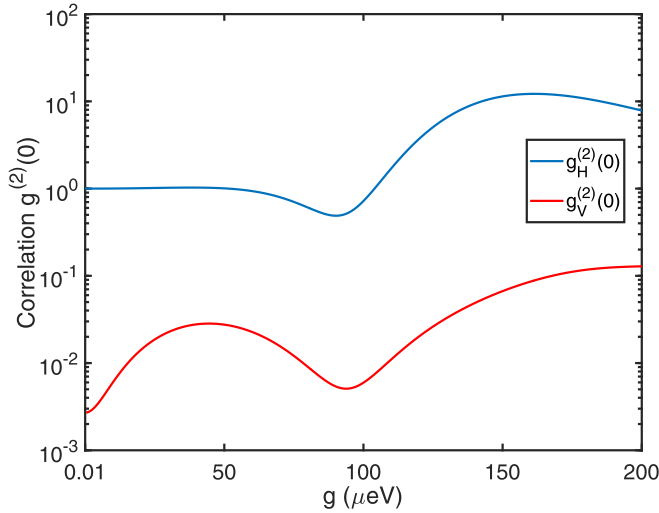


FIG. 8. Semilogarithmic plot of the equal-time second-order intensity correlation functions $g_H^{(2)}(0)$ of the H -polarized photons (upper curve) and $g_V^{(2)}(0)$ of the V -polarized photons (lower curve) as a function of the QD-cavity coupling strength g . The other parameters of the CQED system are $\kappa = 100 \mu\text{eV}$, $\gamma = 0.6 \mu\text{eV}$, $\gamma_H^{dp} = 3 \mu\text{eV}$, $\gamma_V^{dp} = 3 \mu\text{eV}$, $B = 3 \text{ T}$, $\Delta_{CL} = -460 \mu\text{eV}$, $\Delta_{FSS} = 10 \mu\text{eV}$, $\Delta_c = 70 \mu\text{eV}$, $\theta = 20^\circ$, $\delta = 0$, and $\Omega = 10 \mu\text{eV}$.

the magnetic field considered in this paper, a strong photon antibunching effect can be observed in a large part of the region. On the one hand, the minimum value of the second-order intensity correlation function $g_V^{(2)}(0)$ corresponding to the photon blockade can be obtained near $B = 7.3 \text{ T}$, where the order of magnitude of the $g_V^{(2)}(0)$ function is approximately 10^{-4} . On the other hand, the maximum value of the second-order intensity correlation function $g_V^{(2)}(0)$ corresponding to photon-induced tunneling can be obtained near $B = 9.3 \text{ T}$, where the order of magnitude of the V -polarized photon correlation function $g_V^{(2)}(0)$ reaches 10. Based on the above results, we can draw the conclusion that the statistical properties of the V -polarized photons can be manipulated by properly adjusting the external magnetic field B : Not only can photons with an enhanced antibunching effect be obtained, but photons with a strong bunching effect can also be harvested. By tuning the magnetic field we can achieve selective photon blockade statistics. The enhanced photon antibunching effect can be used to generate single-photon sources, which has potential applications in quantum information processing and quantum communication. The photon bunching effect also has potential application prospects in multiphoton lasers [94,95], quantum biology [96,97], metrology [98], and so on. Controllable switching from antibunched to bunched light (or vice versa) can be achieved in such a CQED system, which offers a highly sensitive method to tune photon statistics.

Next, in order to clearly indicate how the QD-cavity coupling strength g affects the photon antibunching for the H -polarized and V -polarized photons, the equal-time second-order intensity correlation functions $g_H^{(2)}(0)$ and $g_V^{(2)}(0)$ versus the QD-cavity coupling strength g are plotted in Fig. 8, respectively. As shown in this figure, the change of the second-order correlation functions $g_H^{(2)}(0)$ and $g_V^{(2)}(0)$ with respect to the coupling strength g exhibits a nonmonotonic behavior. More

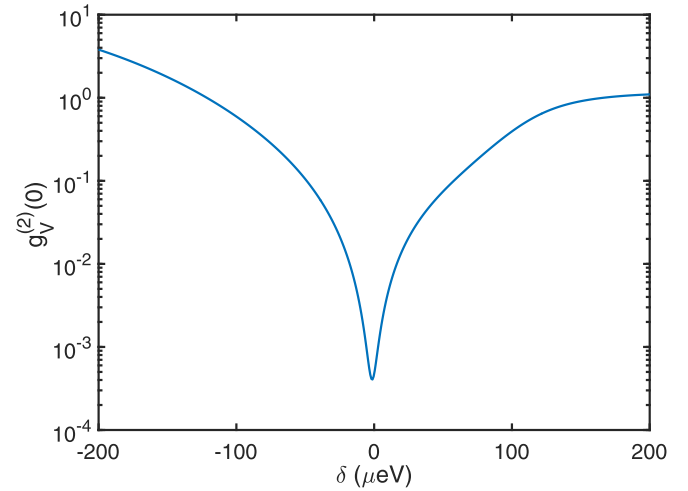


FIG. 9. Semilogarithmic plot of the equal-time second-order intensity correlation function $g_V^{(2)}(0)$ of the V -polarized photons as a function of the detuning δ between the central frequency ω of the two linearly polarized excitons and the central frequency ω_c of the two cavity modes. The other parameters of the CQED system are $\kappa = 100 \mu\text{eV}$, $\gamma = 0.6 \mu\text{eV}$, $\gamma_H^{dp} = 3 \mu\text{eV}$, $\gamma_V^{dp} = 3 \mu\text{eV}$, $B = 3 \text{ T}$, $\Delta_{CL} = -440 \mu\text{eV}$, $\Delta_{FSS} = 10 \mu\text{eV}$, $\Delta_c = 70 \mu\text{eV}$, $\theta = 20^\circ$, $g = 20 \mu\text{eV}$, and $\Omega = 10 \mu\text{eV}$.

specifically, for the H -polarized photons, we find that the photons tend to be coherent for the coupling strength $g \rightarrow 0$, whereas for the V -polarized photons, we observe that the photons tend to be strongly antibunching. The H -polarized photon correlation function $g_H^{(2)}(0)$ decreases with increasing g and arrives at the minimum around the value of $g^{(\text{opt})} = 90 \mu\text{eV}$, corresponding to the minimal value $g_H^{(2)}(0) \simeq 0.49$. With the increase of the QD-cavity coupling strength g above the optimal value $g^{(\text{opt})}$, the value of $g_H^{(2)}(0)$ first increases and then decreases, but it still tends to bunch. The more surprising result, however, is that for the V -polarized photons, the value of the second-order correlation function $g_V^{(2)}(0)$ increases with increasing g in the range of $g \in (0.01, 45) \mu\text{eV}$. Subsequently, the value of $g_V^{(2)}(0)$ decreases first and then increases. It is worth emphasizing that strong photon antibunching effect of the V -polarized photons can be realized effectively in the entire range of g . Based on the above results, we can arrive at the conclusion that for the H -polarized photons, the antibunching effect can only be achieved in the strong-coupling CQED regime, while for V -polarized photons, the strong antibunching effect can be achieved even in the very-weak-coupling CQED regime. The value of the V -polarized photon correlation function $g_V^{(2)}(0)$ has a counterintuitive dependence on the QD-cavity coupling strength g embodied in the phenomenon in which the quality of the photon antibunching is upgraded with decreasing g , which reduces the constraint for a strong interaction between the QD and the cavity. Consequently, the cavity with a high-quality factor is not a necessary precondition to achieve a strong antibunching effect, which increases the possibility of experimental realization.

In all the discussion above, however, our attention has been focused on the condition of resonating the center frequency of the cavity modes with the central frequency of the excitons,

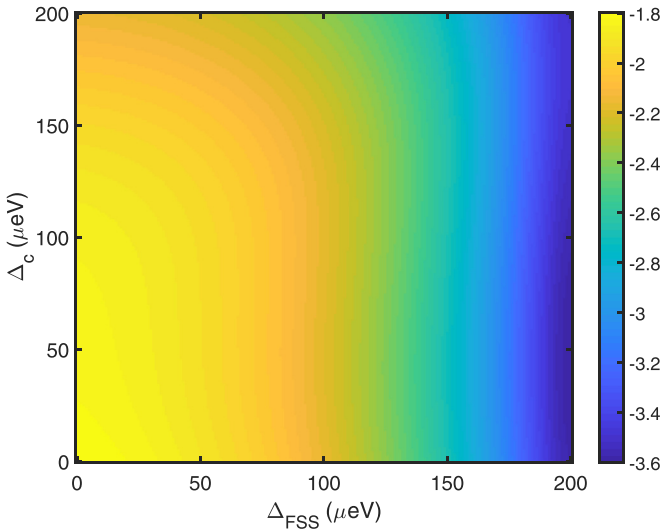


FIG. 10. Logarithmic plot (of base 10) of the equal-time second-order intensity correlation function $g_V^{(2)}(0)$ of the V -polarized photons as a function of the fine-structure splitting of excitons Δ_{FSS} and the splitting of orthogonally polarized cavity modes Δ_c . The system parameters used here are $\kappa = 100 \mu\text{eV}$, $\gamma = 0.6 \mu\text{eV}$, $\gamma_H^{dp} = 3 \mu\text{eV}$, $\gamma_V^{dp} = 3 \mu\text{eV}$, $B = 3 \text{ T}$, $\Delta_{CL} = -460 \mu\text{eV}$, $\theta = 20^\circ$, $g = 20 \mu\text{eV}$, and $\Omega = 10 \mu\text{eV}$.

i.e., $\delta = 0$, yet we have not considered the scenario of the center detuning $\delta \neq 0$ so far. In order to clearly illustrate how the detuning between the cavity modes and the excitons affects the statistical properties of the V -polarized photons, the second-order intensity correlation function $g_V^{(2)}(0)$ versus the center frequency detuning δ is plotted in Fig. 9. It can be seen from Fig. 9 that when the central frequency of the cavity modes is blue detuning from the central frequency of the excitons, the V -polarized photons with bunching effect can be obtained in the range of $\delta \in (-200, -120) \mu\text{eV}$. It is also shown that whether the central frequency of the cavity modes is red detuning or blue detuning to that of the excitons, the strong antibunching effect can be achieved in most regions $\delta \in (-120, 166) \mu\text{eV}$. As a result, the tricky requirement that the QD and the cavity be in resonance or near resonance has been alleviated, which reduces the difficulty of experimental realization.

Finally, to gain further insight, we investigate the contribution of the other system parameters to the statistical properties of the V -polarized photons in the presence of the magnetic field, including the fine-structure splitting of the excitons Δ_{FSS} and the splitting of the orthogonally polarized cavity modes Δ_c . The two-dimensional graph of the second-order intensity correlation function $g_V^{(2)}(0)$ is exhibited on a logarithmic-scale color plot with the fine-structure splitting of the excitons Δ_{FSS} and the splitting of the orthogonally polarized cavity modes Δ_c in Fig. 10. The general trend is that the second-order intensity correlation function $g_V^{(2)}(0)$ decreases with an increase of the exciton fine-structure splitting Δ_{FSS} and the cavity mode splitting Δ_c , which means that the introduction of both the exciton fine-structure splitting and the cavity mode splitting will not significantly reduce the quality of photon antibunching effect. Moreover, it is noteworthy that the V -polarized photons are antibunching in the whole

parameter region selected, which provides a wide range of parameters for the actual experimental implementation and increases the possibility of realizing a single-photon source.

V. CONCLUSION

In summary, we have investigated the possibility of photon statistical control in the solid-state CQED system consisting of a V -level QD embedded in a micropillar cavity via adjusting the external magnetic field. On the one hand, we adopted the quantum master equation approach for numerically calculating the photon occupation number and the second-order intensity correlation function and, furthermore, quantifying its statistical content. On the other hand, starting from a Schrödinger equation approach, an analytical illustration of the second-order correlation function was provided. We found that, on the one hand, when the cavity is driven by the incident H -polarized laser light, the V -polarized photon emissions can appear in the cavity due to the coherent coupling via the term $\Delta_{FSS} \sin \theta \cos \theta (|H\rangle\langle V| + |V\rangle\langle H|)$ and the intermediate modulation of the magnetic field via the term $i\beta(|H\rangle\langle V| - |V\rangle\langle H|)$. On the other hand, we showed that the applied magnetic field plays an important role in modifying the photon statistical properties of the CQED system. Our scheme is based on an operation principle different from previously implemented or proposed photon statistical methods, with the three following major advantages. First of all, by tuning the magnetic field appropriately, the photon statistics properties of the system can be well engineered in the weak-coupling CQED regime and the switching between enhanced photon antibunching and strong photon bunching can be realized. So we can achieve selective photon statistics. Second, our scheme not only makes it possible to control the polarization of photons in the cavity under an external magnetic field, but also enables us to obtain high-transmission photons with a strong antibunching effect. Finally, the photon blockade can be efficiently generated under the nonresonant scenarios but without the need for resonant or near-resonant conditions between the cavity and the QD. The multifrequency photon blockade occurs in the present system, which is different from previous studies on the photon blockade only for specific optical detuning. With these, the relaxation of the strong coupling and resonant or near-resonant conditions between the cavity and the QD increases the possibility of realizing the single-photon sources experimentally.

The realization of the single-photon sources is an important topic in quantum optics because the single-photon sources are fundamental building blocks for quantum information science. The photon blockade effect obtained in the present work offers a possible method to achieve this requirement for the generation and manipulation of single photons within the reach of experimental capabilities. It can provide opportunities for exploring potential applications in light-based quantum technologies [5], including quantum communication, quantum key distribution, quantum networking, and quantum metrology. On the other hand, the design of the quantum device, for example, single-photon transistors [99], crystallization of polaritons [100], all-optical switching [101], and fermionization of photons [102], also relies mainly on the

controlled photon blockade effect. Our scheme, which does not require strong QD-cavity coupling, is a good candidate for the realization of these quantum devices. The present process works with high-quality photon antibunching and bunching over a wide range of parameters, which broadens the realm of quantum optics. We hope that the proposed scheme can provide a possibility for the creation and control of quantum states of electromagnetic radiation.

ACKNOWLEDGMENTS

We gratefully thank the two anonymous referees for their valuable and insightful comments. We also acknowledge

the stimulating discussions with Prof. Xiaoxue Yang and Dr. Rong Yu during the manuscript preparation and further acknowledge contributions to the numerical simulations by Dr. Rong Yu. Two of the authors, S.S. and J.L., are supported partially by the National Natural Science Foundation of China under Grant No. 11675058 and the Fundamental Research Funds for the Central Universities (Huazhong University of Science and Technology) under Grant No. 2018KFYYXJJ037. Y.W. is supported partially by the National Key Research and Development Program of China under Grant No. 2016YFA0301200 as well as the National Natural Science Foundation of China under Grants No. 11875029 and No. 11574104.

-
- [1] T. Yoshie, A. Scherer, J. Hendrickson, G. Khitrova, H. M. Gibbs, G. Rupper, C. Ell, O. B. Shchekin, and D. G. Deppe, Vacuum Rabi splitting with a single quantum dot in a photonic crystal nanocavity, *Nature (London)* **432**, 200 (2004).
- [2] J. P. Reithmaier, G. Sek, A. Löffler, C. Hofmann, S. Kuhn, S. Reitzenstein, L. V. Keldysh, V. D. Kulakovskii, T. L. Reinecke, and A. Forchel, Strong coupling in a single quantum dot–semiconductor microcavity system, *Nature (London)* **432**, 197 (2004).
- [3] B. Lounis and M. Orrit, Single-photon sources, *Rep. Prog. Phys.* **68**, 1129 (2005).
- [4] A. J. Shields, Semiconductor quantum light sources, *Nat. Photon.* **1**, 215 (2007).
- [5] H. J. Kimble, The quantum internet, *Nature (London)* **453**, 1023 (2008).
- [6] V. Scarani, H. B. Pasquinucci, N. J. Cerf, M. Dušek, N. Lütkenhaus, and M. Peev, The security of practical quantum key distribution, *Rev. Mod. Phys.* **81**, 1301 (2009).
- [7] E. M. Purcell, Spontaneous emission probabilities at radio frequencies, *Phys. Rev.* **69**, 37 (1946).
- [8] J. M. Gérard, B. Sermage, B. Gayral, B. Legrand, E. Costard, and V. Thierry-Mieg, Enhanced Spontaneous Emission by Quantum Boxes in a Monolithic Optical Microcavity, *Phys. Rev. Lett.* **81**, 1110 (1998).
- [9] M. Brune, F. Schmidt-Kaler, A. Maali, J. Dreyer, E. Hagley, J. M. Raimond, and S. Haroche, Quantum Rabi Oscillation: A Direct Test of Field Quantization in a Cavity, *Phys. Rev. Lett.* **76**, 1800 (1996).
- [10] R. J. Thompson, G. Rempe, and H. J. Kimble, Observation of Normal-Mode Splitting for an Atom in an Optical Cavity, *Phys. Rev. Lett.* **68**, 1132 (1992).
- [11] M. O. Scully and M. S. Zubairy, *Quantum Optics* (Cambridge University Press, Cambridge, 1997).
- [12] J. M. Fink, M. Göppl, M. Baur, R. Bianchetti, P. J. Leek, A. Blais, and A. Wallraff, Climbing the Jaynes-Cummings ladder and observing its \sqrt{n} nonlinearity in a cavity QED system, *Nature (London)* **454**, 315 (2008).
- [13] J. Kasprzak, S. Reitzenstein, E. A. Muljarov, C. Kistner, C. Schneider, M. Strauss, S. Höfling, A. Forchel, and W. Langbein, Up on the Jaynes-Cummings ladder of a quantum-dot/microcavity system, *Nat. Mater.* **9**, 304 (2010).
- [14] A. Faraon, I. Fushman, D. Englund, N. Stoltz, P. Petroff, and J. Vučković, Coherent generation of non-classical light on a chip via photon-induced tunneling and blockade, *Nat. Phys.* **4**, 859 (2008).
- [15] B. Dayan, A. S. Parkins, T. Aoki, E. P. Ostby, K. J. Vahala, and H. J. Kimble, A photon turnstile dynamically regulated by one atom, *Science* **319**, 1062 (2008).
- [16] K. M. Birnbaum, A. Boca, R. Miller, A. D. Boozer, T. E. Northup, and H. J. Kimble, Photon blockade in an optical cavity with one trapped atom, *Nature (London)* **436**, 87 (2005).
- [17] Y.-x. Liu, A. Miranowicz, Y. B. Gao, J. Bajer, C. P. Sun, and F. Nori, Qubit-induced phonon blockade as a signature of quantum behavior in nanomechanical resonators, *Phys. Rev. A* **82**, 032101 (2010).
- [18] A. Reinhard, T. Volz, M. Winger, A. Badolato, K. J. Hennessy, E. L. Hu, and A. Imamoglu, Strongly correlated photons on a chip, *Nat. Photon.* **6**, 93 (2012).
- [19] T. Peyronel, O. Firstenberg, Q.-Y. Liang, S. Hofferberth, A. V. Gorshkov, T. Pohl, M. D. Lukin, and V. Vuletić, Quantum nonlinear optics with single photons enabled by strongly interacting atoms, *Nature (London)* **488**, 57 (2012).
- [20] K. Müller, A. Rundquist, K. A. Fischer, T. Sarmiento, and K. G. Lagoudakis, Coherent Generation of Nonclassical Light on Chip via Detuned Photon Blockade, *Phys. Rev. Lett.* **114**, 233601 (2015).
- [21] C. Lang, D. Bozyigit, C. Eichler, L. Steffen, J. M. Fink, A. A. Abdumalikov, Jr., M. Baur, S. Filipp, M. P. da Silva, A. Blais, and A. Wallraff, Observation of Resonant Photon Blockade at Microwave Frequencies Using Correlation Function Measurements, *Phys. Rev. Lett.* **106**, 243601 (2011).
- [22] A. J. Hoffman, S. J. Srinivasan, S. Schmidt, L. Spietz, J. Aumentado, H. E. Türeci, and A. A. Houck, Dispersive Photon Blockade in a Superconducting Circuit, *Phys. Rev. Lett.* **107**, 053602 (2011).
- [23] J. Bourassa, F. Beaudoin, J. M. Gambetta, and A. Blais, Josephson-junction-embedded transmission-line resonators: From Kerr medium to in-line transmon, *Phys. Rev. A* **86**, 013814 (2012).
- [24] Y.-x. Liu, X.-W. Xu, A. Miranowicz, and F. Nori, From blockade to transparency: Controllable photon transmission through a circuit-QED system, *Phys. Rev. A* **89**, 043818 (2014).
- [25] J. T. Shen and S. H. Fan, Strongly Correlated Two-Photon Transport in a One-Dimensional Waveguide Coupled to a Two-Level System, *Phys. Rev. Lett.* **98**, 153003 (2007).

- [26] S. Mahmoodian, M. Čepulkovskis, S. Das, P. Lodahl, K. Hammerer, and A. S. Sørensen, Strongly Correlated Photon Transport in Waveguide Quantum Electrodynamics with Weakly Coupled Emitters, *Phys. Rev. Lett.* **121**, 143601 (2018).
- [27] J. T. Shen and S. H. Fan, Strongly correlated multiparticle transport in one dimension through a quantum impurity, *Phys. Rev. A* **76**, 062709 (2007).
- [28] P. Rabl, Photon Blockade Effect in Optomechanical Systems, *Phys. Rev. Lett.* **107**, 063601 (2011).
- [29] X.-Y. Lü, W.-M. Zhang, S. Ashhab, Y. Wu, and F. Nori, Quantum-criticality-induced strong Kerr nonlinearities in optomechanical systems, *Sci. Rep.* **3**, 2943 (2013).
- [30] J. Q. Liao and C. K. Law, Correlated two-photon scattering in cavity optomechanics, *Phys. Rev. A* **87**, 043809 (2013).
- [31] X. W. Xu, Y. J. Li, and Y. X. Liu, Photon-induced tunneling in optomechanical systems, *Phys. Rev. A* **87**, 025803 (2013).
- [32] M. Ludwig, A. H. Safavi-Naeini, O. Painter, and F. Marquardt, Enhanced Quantum Nonlinearities in a Two Mode Optomechanical System, *Phys. Rev. Lett.* **109**, 063601 (2012).
- [33] A. Kronwald, M. Ludwig, and F. Marquardt, Full photon statistics of a light beam transmitted through an optomechanical system, *Phys. Rev. A* **87**, 013847 (2013).
- [34] K. Stannigel, P. Komar, S. J. M. Habraken, S. D. Bennett, M. D. Lukin, P. Zoller, and P. Rabl, Optomechanical Quantum Information Processing with Photons and Phonons, *Phys. Rev. Lett.* **109**, 013603 (2012).
- [35] J. Q. Liao and F. Nori, Photon blockade in quadratically coupled optomechanical systems, *Phys. Rev. A* **88**, 023853 (2013).
- [36] D. Hu, S.-Y. Huang, J.-Q. Liao, L. Tian, and H.-S. Goan, Quantum coherence in ultrastrong optomechanics, *Phys. Rev. A* **91**, 013812 (2015).
- [37] H. Xie, C.-G. Liao, X. Shang, M.-Y. Ye, and X.-M. Lin, Phonon blockade in a quadratically coupled optomechanical system, *Phys. Rev. A* **96**, 013861 (2017).
- [38] G. L. Zhu, X.-Y. Lü, L. L. Wan, T. S. Yin, Q. Bin, and Y. Wu, Controllable nonlinearity in a dual-coupling optomechanical system under a weak-coupling regime, *Phys. Rev. A* **97**, 033830 (2018).
- [39] R. Huang, A. Miranowicz, J.-Q. Liao, F. Nori, and H. Jing, Nonreciprocal Photon Blockade, *Phys. Rev. Lett.* **121**, 153601 (2018).
- [40] B. Li, R. Huang, X.-W. Xu, A. Miranowicz, and H. Jing, Nonreciprocal unconventional photon blockade in a spinning optomechanical system, *Photon. Res.* **7**, 630 (2019).
- [41] Y. H. Zhou, H. Z. Shen, X. Y. Zhang, and X. X. Yi, Zero eigenvalues of a photon blockade induced by a non-Hermitian Hamiltonian with a gain cavity, *Phys. Rev. A* **97**, 043819 (2018).
- [42] T. C. H. Liew and V. Savona, Single Photons from Coupled Quantum Modes, *Phys. Rev. Lett.* **104**, 183601 (2010).
- [43] M. Bamba, A. Imamoğlu, I. Carusotto, and C. Ciuti, Origin of strong photon antibunching in weakly nonlinear photonic molecules, *Phys. Rev. A* **83**, 021802(R) (2011).
- [44] A. Majumdar and D. Gerace, Single-photon blockade in doubly resonant nanocavities with second-order nonlinearity, *Phys. Rev. B* **87**, 235319 (2013).
- [45] H. Flayac and V. Savona, Input-output theory of the unconventional photon blockade, *Phys. Rev. A* **88**, 033836 (2013).
- [46] S. Ferretti, V. Savona, and D. Gerace, Optimal antibunching in passive photonic devices based on coupled nonlinear resonators, *New J. Phys.* **15**, 025012 (2013).
- [47] D. Gerace and V. Savona, Unconventional photon blockade in doubly resonant microcavities with second-order nonlinearity, *Phys. Rev. A* **89**, 031803(R) (2014).
- [48] H. Flayac, D. Gerace, and V. Savona, An all-silicon single-photon source by unconventional photon blockade, *Sci. Rep.* **5**, 11223 (2015).
- [49] H. Flayac and V. Savona, Unconventional photon blockade, *Phys. Rev. A* **96**, 053810 (2017).
- [50] X.-W. Xu and Y. Li, Tunable photon statistics in weakly nonlinear photonic molecules, *Phys. Rev. A* **90**, 043822 (2014).
- [51] H. Flayac and V. Savona, Single photons from dissipation in coupled cavities, *Phys. Rev. A* **94**, 013815 (2016).
- [52] F. Zou, D.-G. Lai, and J.-Q. Liao, Photon blockade effect in a coupled cavity system, [arXiv:1803.06642](https://arxiv.org/abs/1803.06642).
- [53] Y. H. Zhou, H. Z. Shen, and X. X. Yi, Unconventional photon blockade with second-order nonlinearity, *Phys. Rev. A* **92**, 023838 (2015).
- [54] C. Vaneph, A. Morvan, G. Aiello, M. Féchant, M. Aprili, J. Gabelli, and J. Estève, Observation of the Unconventional Photon Blockade Effect in the Microwave Domain, *Phys. Rev. Lett.* **121**, 043602 (2018).
- [55] A. Miranowicz, J. Bajer, N. Lambert, Y.-x. Liu, and F. Nori, Tunable multiphonon blockade in coupled nanomechanical resonators, *Phys. Rev. A* **93**, 013808 (2016).
- [56] B. Sarma and A. K. Sarma, Unconventional photon blockade in three-mode optomechanics, *Phys. Rev. A* **98**, 013826 (2018).
- [57] L.-L. Zheng, T.-S. Yin, Q. Bin, X.-Y. Lü, and Y. Wu, Single-photon-induced phonon blockade in a hybrid spin-optomechanical system, *Phys. Rev. A* **99**, 013804 (2019).
- [58] H. Xie, C.-G. Liao, X. Shang, Z.-H. Chen, and X.-M. Lin, Optically induced phonon blockade in an optomechanical system with second-order nonlinearity, *Phys. Rev. A* **98**, 023819 (2018).
- [59] D.-Y. Wang, C.-H. Bai, S. Liu, S. Zhang, and H.-F. Wang, Distinguishing photon blockade in a \mathcal{PT} -symmetric optomechanical system, *Phys. Rev. A* **99**, 043818 (2019).
- [60] H. J. Snijders, J. A. Frey, J. Norman, H. Flayac, V. Savona, A. C. Gossard, J. E. Bowers, M. P. van Exter, D. Bouwmeester, and W. Löffler, Observation of the Unconventional Photon Blockade, *Phys. Rev. Lett.* **121**, 043601 (2018).
- [61] A. Majumdar, M. Bajcsy, A. Rundquist, and J. Vučković, Loss-Enabled Sub-Poissonian Light Generation in a Bimodal Nanocavity, *Phys. Rev. Lett.* **108**, 183601 (2012).
- [62] J. Tang, W. D. Geng, and X. L. Xu, Quantum interference induced photon blockade in a coupled single quantum dot-cavity system, *Sci. Rep.* **5**, 9252 (2015).
- [63] Y. L. Liu, G. Z. Wang, Y.-x. Liu, and F. Nori, Mode coupling and photon antibunching in a bimodal cavity containing a dipole quantum emitter, *Phys. Rev. A* **93**, 013856 (2016).
- [64] J. P. Xu, S. L. Chang, Y. P. Yang, S. Y. Zhu, and G. S. Agarwal, Hyperradiance accompanied by nonclassicality, *Phys. Rev. A* **96**, 013839 (2017).

- [65] J. H. Li, C. L. Ding, and Y. Wu, Enhanced photon antibunching via interference effects in a Δ configuration, *Phys. Rev. A* **100**, 033814 (2019).
- [66] A. Laucht, F. Hofbauer, N. Hauke, J. Angele, S. Stobbe, M. Kaniber, G. Böhm, P. Lodahl, M. C. Amann, and J. J. Finley, Electrical control of spontaneous emission and strong coupling for a single quantum dot, *New J. Phys.* **11**, 023034 (2009).
- [67] C. Kistner, T. Heindel, C. Schneider, A. Rahimi-Iman, S. Reitzenstein, S. Höfling, and A. Forchel, Demonstration of strong coupling via electro-optical tuning in high-quality QD-micropillar systems, *Opt. Express* **16**, 15006 (2008).
- [68] K. Hennessy, A. Badolato, M. Winger, D. Gerace, M. Atatüre, S. Gulde, S. Fält, E. L. Hu, and A. Imamoglu, Quantum nature of a strongly coupled single quantum dot-cavity system, *Nature (London)* **445**, 896 (2007).
- [69] S. Reitzenstein, S. Münch, P. Franek, A. Rahimi-Iman, A. Löffler, S. Höfling, L. Worschech, and A. Forchel, Control of the Strong Light-Matter Interaction between an Elongated $\text{In}_{0.3}\text{Ga}_{0.7}\text{As}$ Quantum Dot and a Micropillar Cavity using External Magnetic Fields, *Phys. Rev. Lett.* **103**, 127401 (2009).
- [70] H. Kim, T. C. Shen, D. Sridharan, G. S. Solomon, and E. Waks, Magnetic field tuning of a quantum dot strongly coupled to a photonic crystal cavity, *Appl. Phys. Lett.* **98**, 091102 (2011).
- [71] Q. J. Ren, J. Lu, H. H. Tan, S. Wu, L. X. Sun, W. H. Zhou, W. Xie, Z. Sun, Y. Y. Zhu, C. Jagadish, S. C. Shen, and Z. H. Chen, Spin-resolved Purcell effect in a quantum dot microcavity system, *Nano Lett.* **12**, 3455 (2012).
- [72] A. Kuther, M. Bayer, A. Forchel, A. Gorbunov, V. B. Timofeev, F. Schäfer, and J. P. Reithmaier, Zeeman splitting of excitons and biexcitons in single $\text{In}_{0.60}\text{Ga}_{0.40}\text{As}/\text{GaAs}$ self-assembled quantum dots, *Phys. Rev. B* **58**, R7508 (1998).
- [73] M. Bayer, G. Ortner, O. Stern, A. Kuther, A. A. Gorbunov, A. Forchel, P. Hawrylak, S. Fafard, K. Hinzer, T. L. Reinecke, S. N. Walck, J. P. Reithmaier, F. Klopff, and F. Schäfer, Fine structure of neutral and charged excitons in self-assembled $\text{In}(\text{Ga})\text{As}/(\text{Al})\text{GaAs}$ quantum dots, *Phys. Rev. B* **65**, 195315 (2002).
- [74] A. Majumdar, P. Kaer, M. Bajcsy, E. D. Kim, K. G. Lagoudakis, A. Rundquist, and J. Vučković, Proposed Coupling of an Electron Spin in a Semiconductor Quantum Dot to a Nanosize Optical Cavity, *Phys. Rev. Lett.* **111**, 027402 (2013).
- [75] S. Reitzenstein, S. Münch, P. Franek, A. Löffler, S. Höfling, L. Worschech, A. Forchel, I. V. Ponomarev, and T. L. Reinecke, Exciton spin state mediated photon-photon coupling in a strongly coupled quantum dot microcavity system, *Phys. Rev. B* **82**, 121306 (2010).
- [76] V. Giesz, N. Somaschi, G. Hornecker, T. Grange, B. Reznichenko, L. De Santis, J. Demory, C. Gomez, I. Sagnes, A. Lemaître, O. Krebs, N. D. Lanzillotti-Kimura, L. Lanco, A. Auffèves, and P. Senellart, Coherent manipulation of a solid-state artificial atom with few photons, *Nat. Commun.* **7**, 11986 (2016).
- [77] L. D. Santis, C. Antón, B. Reznichenko, N. Somaschi, G. Coppola, J. Senellart, C. Gómez, A. Lemaître, I. Sagnes, A. G. White, L. Lanco, A. Auffèves, and P. Senellart, A solid-state single-photon filter, *Nat. Nanotechnol.* **12**, 663 (2017).
- [78] C. Antón, P. Hilaire, C. A. Kessler, J. Demory, C. Gómez, A. Lemaître, I. Sagnes, N. D. Lanzillotti-Kimura, O. Krebs, N. Somaschi, P. Senellart, and L. Lanco, Tomography of the optical polarization rotation induced by a single quantum dot in a cavity, *Optica* **4**, 1326 (2017).
- [79] H. Snijders, J. A. Frey, J. Norman, V. P. Post, A. C. Gossard, J. E. Bowers, M. P. van Exter, W. Löffler, and D. Bouwmeester, Fiber-Coupled Cavity-QED Source of Identical Single Photons, *Phys. Rev. Appl.* **9**, 031002 (2018).
- [80] H. Snijders, J. A. Frey, J. Norman, M. P. Bakker, E. C. Langman, A. Gossard, J. E. Bowers, M. P. van Exter, D. Bouwmeester, and W. Löffler, Purification of a single-photon nonlinearity, *Nat. Commun.* **7**, 12578 (2016).
- [81] M. P. Bakker, A. V. Barve, T. Ruytenberg, W. Löffler, L. A. Coldren, D. Bouwmeester, and M. P. van Exter, Polarization degenerate solid-state cavity quantum electrodynamics, *Phys. Rev. B* **91**, 115319 (2015).
- [82] H. Eleuch, Quantum trajectories and autocorrelation function in semiconductor microcavity, *Appl. Math. Inform. Sci.* **3**, 185 (2009); Autocorrelation function of microcavity-emitting field in the linear regime, *Eur. Phys. J. D* **48**, 139 (2008); H. Eleuch, and N. Rachid, Autocorrelation function of microcavity-emitting field in the non-linear regime, *ibid.* **57**, 259 (2010); H. Eleuch, Entanglement and autocorrelation function in semiconductor microcavities, *Int. J. Mod. Phys. B* **24**, 5653 (2010).
- [83] H. Eleuch, Photon statistics of light in semiconductor microcavities, *J. Phys. B* **41**, 055502 (2008).
- [84] K. Hennessy, C. Högerle, E. Hu, A. Badolato, and A. Imamoglu, Tuning photonic nanocavities by atomic force microscope nano-oxidation, *Appl. Phys. Lett.* **89**, 041118 (2006).
- [85] C. Jiménez-Orjuela, H. Vinck-Posada, and J. M. Villas-Bôas, Dark excitons in a quantum-dot-cavity system under a tilted magnetic field, *Phys. Rev. B* **96**, 125303 (2017).
- [86] Q. Mermillod, D. Wigger, V. Delmonte, D. E. Reiter, C. Schneider, M. Kamp, S. Höfling, W. Langbein, T. Kuhn, G. Nogues, and J. Kasprzak, Dynamics of excitons in individual InAs quantum dots revealed in four-wave mixing spectroscopy, *Optica* **3**, 377 (2016).
- [87] W. Zhang, Z. Yu, Y. Liu, and Y. Peng, Optical nonlinearity in a quantum dot-microcavity system under an external magnetic field, *J. Opt. Soc. Am. B* **31**, 296 (2014).
- [88] C. A. Jiménez-Orjuela, H. Vinck-Posada, and J. M. Villas-Bôas, Polarization switch in an elliptical micropillar-quantum dot system induced by a magnetic field in Faraday configuration, *Phys. Lett. A* **382**, 3216 (2018).
- [89] J. H. Li, S. T. Shen, Y. Qu, D. Zhang, and Y. Wu, Generating orthogonally polarized dual frequency combs with slow megahertz repetition rates by a low-nanowatt-level pump, *Phys. Rev. A* **98**, 023848 (2018).
- [90] P. Machnikowski, Theory of two-photon processes in quantum dots: Coherent evolution and phonon-induced dephasing, *Phys. Rev. B* **78**, 195320 (2008).
- [91] G. S. Agarwal, *Quantum Optics* (Cambridge University Press, Cambridge, 2013).
- [92] J. H. Li and Y. Wu, Quality of photon antibunching in two cavity-waveguide arrangements on a chip, *Phys. Rev. A* **98**, 053801 (2018).
- [93] W. Zhang, Z. Yu, Y. Liu, and Y. Peng, Optimal photon antibunching in a quantum-dot-bimodal-cavity system, *Phys. Rev. A* **89**, 043832 (2014).
- [94] D. J. Gauthier, Q. L. Wu, S. E. Morin, and T. W. Mossberg, Realization of a Continuous-Wave, Two-Photon Optical Laser, *Phys. Rev. Lett.* **68**, 464 (1992).

- [95] Q. Bin, X.-Y. Lü, F. P. Laussy, F. Nori, and Y. Wu, N -phonon bundle emission via the anti-Stokes process, [arXiv:1907.12714](https://arxiv.org/abs/1907.12714).
- [96] W. Denk, J. Strickler, and W. Webb, Two-photon laser scanning fluorescence microscopy, *Science* **248**, 73 (1990).
- [97] N. G. Horton, K. Wang, D. Kibat, C. G. Clark, F. W. Wise, C. B. Schaffer, and C. Xu, *In vivo* three-photon microscopy of subcortical structures within an intact mouse brain, *Nat. Photon.* **7**, 205 (2013).
- [98] I. Afek, O. Ambar, and Y. Silberberg, High-NOON states by mixing quantum and classical light, *Science* **328**, 879 (2010).
- [99] F.-Y. Hong and S.-J. Xiong, Single-photon transistor using microtoroidal resonators, *Phys. Rev. A* **78**, 013812 (2008).
- [100] M. J. Hartmann, Polariton Crystallization in Driven Arrays of Lossy Nonlinear Resonators, *Phys. Rev. Lett.* **104**, 113601 (2010).
- [101] T. Volz, A. Reinhard, M. Winger, A. Badolato, K. J. Hennessy, E. L. Hu, and A. Imamoglu, Ultrafast all-optical switching by single photons, *Nat. Photon.* **6**, 605 (2012).
- [102] I. Carusotto, D. Gerace, H. E. Tureci, S. De Liberato, C. Ciuti, and A. Imamoglu, Fermionized Photons in an Array of Driven Dissipative Nonlinear Cavities, *Phys. Rev. Lett.* **103**, 033601 (2009).